Agricultural and Forest Meteorology 232 (2017) 74–88

Contents lists available at ScienceDirect

Agricultural and Forest Meteorology

journal homepage: www.elsevier.com/locate/agrformet

Retrieval of seasonal Rubisco-limited photosynthetic capacity at global FLUXNET sites from hyperspectral satellite remote sensing: Impact on carbon modelling

Paul B. Alton

Department of Geography, Swansea University, SA2 8PP, UK

ARTICLE INFO

Article history:
Received 12 January 2016
Received in revised form 18 July 2016
Accepted 4 August 2016

Keywords:
Carbon cycle
Land-surface modelling
Photosynthetic capacity
Moderate Resolution Imaging Spectroradiometer (MODIS)
FLUXNET
MEdium Resolution Imaging Spectrometer (MERIS)

ABSTRACT

Process-based ecophysiological models, which simulate carbon exchange at the land-surface, are powerful and indispensable tools for understanding how vegetation behaves under present and future climate. However, these models are necessarily complex, containing numerous biophysical parameters which are often poorly defined. The current study develops a novel retrieval of Rubisco-limited top-of-canopy photosynthetic capacity (i.e. maximum carboxylation rate, $V_{cmax}^{25,toc}$), which is one of the most critical parameters in the calculation of Gross Primary Productivity (GPP). The retrieval combines standard remote sensing satellite products of Leaf Area Index (LAI), from the Moderate Resolution Imaging Spectroradiometer (MODIS), with a hyperspectral index of total canopy chlorophyll concentration from the MEdium Resolution Imaging Spectrometer (MERIS). Monthly values of $V_{cmax}^{25,toc}$ are determined over a 9 year period for 296 global FLUXNET sites (catalogue made available online) and 8 Plant Functional Types (PFTs). PFT averages agree favourably with compilations of field-based measurements. However, according to a Monte Carlo analysis, our method is still currently subject to large systematic uncertainties (25–30%), much of which arises from the empirical relationship between maximum electron transport and leaf chlorophyll content. For all 8 PFTs, except tropical broadleaf forest, $V_{cmax}^{25,toc}$ varies considerably across the season (generally a factor of 1.6). Similarly, variability between sites of the same PFT is significant (interquartile range is 40% of the median). This suggests an important additional role for satellites in the spatial and temporal parameterisation of carbon models. Inclusion of this temporal and spatial variability in a process-based ecophysiological model produces, respectively, an impact of 11% and 12% on simulated GPP.

1. Introduction

Process-based ecophysiological Land-Surface Models (LSMs) offer a means of simulating and understanding carbon, water and energy exchange between the vegetated land-surface and the atmosphere. They are, therefore, an important tool for predicting how vegetation classes or PFTs (see Table 1 for frequent acronyms) will respond to environmental change (e.g. Running et al., 1999; Friend et al., 2007; IPCC, 2013; Sato et al., 2015). By reason of their complexity, these mechanistic models (e.g. LPJ, CLM and SiB; Sellers et al., 1996; Zaehle et al., 2005; Bonan et al., 2011), require a large number of parameters, many of which must be defined for several PFTs. This makes the calibration of such models, against eddy covariance fluxes for example, an under-determined problem (Medlyn et al., 2005). One solution is to adopt models of lesser complexity such as light-use efficiency algorithms (McCallum et al., 2009) but understanding and simulating the underlying physiological mechanisms is becoming increasingly important to make reliable predictions under climate change. Another solution is to assimilate a greater number of field-based and remotely sensed observations of vegetation biophysical parameters (Williams et al., 2009; Richardson et al., 2010).

For ecophysiological LSMs, probably the most important parameter is the maximum carboxylation rate or Rubisco-limited photosynthetic capacity, usually defined at a standard temperature of 25 °C (V_{cmax}^{25}; Dang et al., 1998; Bonan et al., 2011). V_{cmax}^{25} enters a biochemical co-limitation submodel for photosynthesis (Farquhar et al., 1980; Collatz et al., 1991). V_{cmax}^{25} is inferred for many species from leaf measurements of photosynthesis using a light chamber. However, a large variation appears to exist: (i) vertically through the canopy (Carswell et al., 2000; Lewis et al., 2000; Meir et al., 2002); (ii) across the growing season (Wilson et al., 2000; Grassi

E-mail address: p.alton@swansea.ac.uk

http://dx.doi.org/10.1016/j.agrformet.2016.08.001
0168-1923/

Table 1
An alphabetical list of acronyms, abbreviations and quantities used frequently in the main text. Units are given where appropriate.

	Definition
$Chl(L)$	Leaf chlorophyll content ($g\,m^{-2}$)
GPP	Gross Primary Productivity ($kg\,m^{-2}\,yr^{-1}$)
J^{25}_{max}	Maximum electron transport rate at 25 °C ($\mu mol\,m^{-2}\,s^{-1}$)
LAI	Leaf Area Index ($m^2\,m^{-2}$)
LSM	Land Surface Model
MERIS	MEdium Resolution Imaging Spectrometer
MODIS	Moderate Resolution Imaging Spectroradiometer
MTCI	MERIS Terrestrial Chlorophyll Index
N	Nitrogen
PFT	Plant Functional Type
V^{25}_{cmax}	Maximum carboxylation rate ($\mu mol\,m^{-2}\,s^{-1}$) (Rubisco-limited photosynthetic capacity)
$V^{25,toc}_{cmax}$	V^{25}_{cmax} at canopy top ($\mu mol\,m^{-2}\,s^{-1}$)
$V^{25,toc}_{cmax}(site, month)$	site average seasonal cycle of $V^{25,toc}_{cmax}$ ($\mu mol\,m^{-2}\,s^{-1}$)
$V^{25,toc}_{cmax}(pft, month)$	PFT average seasonal cycle of $V^{25,toc}_{cmax}$ ($\mu mol\,m^{-2}\,s^{-1}$)

et al., 2005); and (iii) for canopies within the same PFT (Wright et al., 2005; Kattge et al., 2009). The temporal variation is noted as a cause of error in carbon models (Wilson et al., 2001; Xu and Baldocchi, 2003; Bonan et al., 2011). While some land surface and carbon models assume a vertical decline in active (chlorophyll plus Rubisco) leaf nitrogen (N; Chen et al., 1993; Schulze et al., 1994; Friend, 2001; Bonan et al., 2011), very few take account of either seasonal (temporal) or sub-PFT (spatial) variability. In particular, global carbon models typically assume a constant V^{25}_{cmax} for each PFT throughout the year (Kattge et al., 2009), although leaf photosynthesis itself is reduced by impairment ("stress") factors for temperature, humidity deficit and soil moisture availability (Sellers et al., 1996).

In a few cases, seasonal V^{25}_{cmax} is measured at individual sites from leaf measurements and implemented in a model which is then better at reproducing observed carbon eddy covariance fluxes (Wilson et al., 2001). Similarly, models that reduce V^{25}_{cmax} according to daylength, based on some evidence from the field (Bauerle et al., 2012), perform more convincingly early and late in the season against fluxes (Bonan et al., 2011; Medvigy et al., 2013). This empirical approach, though convenient, is probably oversimplistic and also neglects spatial (sub-PFT) variability in V^{25}_{cmax}. Alton (2011) crudely attempts to introduce 1° spatial heterogeneity of V^{25}_{cmax} into a global simulation of net primary productivity by assuming a simple proportionality between the hyperspectral reflectance index MTCI (discussed below) and photosynthetic capacity. Mean V^{25}_{cmax} for each PFT is calibrated by inverting an LSM against observed carbon site fluxes. Although the simulation neglects seasonal variabilty, it does produce one of the first global maps of average growing season V^{25}_{cmax} based on remote sensing. The current study extends this approach.

In some cases, V^{25}_{cmax} is retrieved for individual FLUXNET sites from net ecosystem carbon fluxes measured with eddy covariance (Reichstein et al., 2003; Wang et al., 2007). However, parameter-colinearity means that retrieved values depend on assumed values for other (e.g. respiration) parameters, which themselves are highly uncertain (Abramowitz et al., 2008; Medlyn et al., 2005). Evidently, greater data inputs are required to the modelling process.

In this context, measurements of photosynthetic capacity from space, using remote sensing of canopy reflectance, would be a major advance in constraining ecophysiological processed-based LSMs, particularly if we are to allow for temporal and sub-PFT variability in key parameters. Established remote sensing techniques of broadband reflectance, particularly in the form of vegetation indices, provide essential measures of leaf cover and the fraction of photosynthetically-active radiation absorbed by vegetation during photosynthesis (e.g. Los et al., 2000). Recently, though, Houborg et al. (2013) use broadband reflectance to infer chlorophyll leaf content, although hyperspectral measurements, in addition to broadband reflectance, are probably needed to avoid inferring too many biophysical properties from too few observations (Combal et al., 2003).

The recent availability of aircraft and satellite hyperspectral instruments allows a few pioneering attempts to relate narrow-band reflectance to photosynthetic activity and leaf N content. Hyperspectral studies fall into two main categories: (1) the correlation of a large number of narrow waveband optical and near-infrared radiances to leaf chemistry, including N content; and (2) the analysis of a small number of wavelengths associated with a specific spectral feature such as chlorophyll absorption. We treat these two groups in turn.

Smith et al. (2002) use partial least squares regressions (a kind of eigenvector analysis) to successfully regress ($R^2 \simeq 0.8$) the hyperspectral response over 0.2–2.4 μm of the Airborne Visible/Infrared Imaging Spectrometer (AVIRIS) to whole canopy N. Further, the authors show that canopy total N correlates strongly ($R^2 \simeq 0.8$) to above-ground net primary productivity in extensive temperate broadleaf and needleleaf forests (see also Ollinger et al., 2013). Both Serbin et al. (2012) and Doughty et al. (2011) demonstrate that *in situ* measurements of leaf reflectance and transmittance correlate moderately well with J^{25}_{max} and V^{25}_{cmax} which offers promise to remote sensing of canopy photosynthetic capacity. However, it is important to note that that these aforementioned studies combine a large number of narrow wavebands (up to 44 in Serbin et al., 2012) in a purely empirical fashion with less reliance on understanding the underlying mechanisms giving rise to the spectral features.

A second group of hyperspectral work focusses on a specific absorption/reflection feature and uses far fewer wavelengths. The Photochemical Reflectance Index, at 531 nm, correlates moderately strongly with the conversion of absorbed sunlight into canopy-assimilated carbon and, as such, provides a useful parameterisation for light-use efficiency algorithms (Yuan et al., 2007; McCallum et al., 2009) as opposed to Farquhar-type ecophysiological LSMs which contain explicit formulations of J^{25}_{max} and V^{25}_{cmax}. In another approach, Zhang et al. (2014) combine sun-induced fluorescence (715–758 nm) with other broadband and hyperspectral indices to infer leaf chlorophyll content at several crop sites, which is then assimilated into a canopy radiative transfer and carbon model to determine V^{25}_{cmax}.

At leaf level, Middleton et al. (2003) conclude that the red-edge derivative, i.e. the steep gradient in spectral reflectance between the red and near-infrared domains (690–750 nm), provides the strongest probe of foliar chemistry such as chlorophyll content. This is exploited in the Medium Resolution Imaging Spectrometer (MERIS) Terrestrial Chlorophyll Index (MTCI):

$$MTCI = \frac{R_{753.75} - R_{708.75}}{R_{708.75} - R_{681.25}} \quad (1)$$

where R is reflectance at the subscript wavelength given in nanometres (Curran et al., 2007). The filters are narrow (Fig. 1) to quantify the gradient in the red-edge which is known to correlate strongly ($R^2 = 0.6–0.8$) with canopy chlorophyll concentration over crops and the chlorophyll content of broadleaves and needleleaves (Dash and Curran, 2007; Dash et al., 2010) studied in the laboratory. Thus far, the implementation of MTCI in carbon modelling is very limited, although Boyd et al. (2012) demonstrate a fair correlation between GPP and MTCI at 30 FLUXNET sites ($R^2 \leq 0.9$).

In the current study, we infer canopy chlorophyll concentration at 296 global FLUXNET sites from the standard MTCI product. The canopy chlorophyll content is then related to J^{25}_{max} which, itself, is known to correlate quite tightly, through a frequently observed optimisation of active leaf N, with V^{25}_{cmax} (e.g. Wullschleger, 1993; Meir et al., 2002; Walker et al., 2014). The long-term objective is

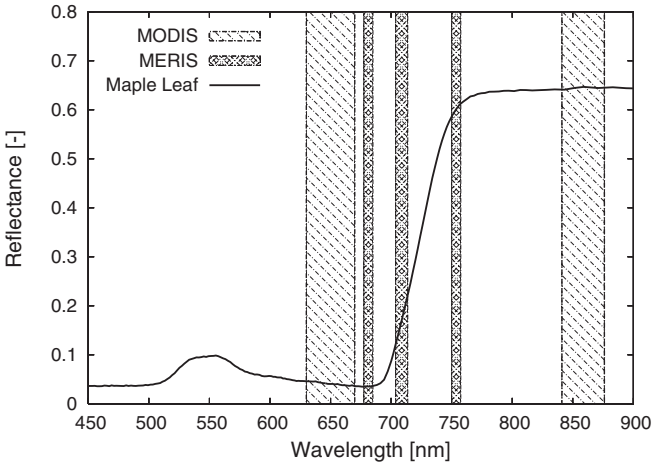

Fig. 1. Hyperspectral MERIS filters (doubled hashed area), used for the MTCI index, compared against the broadband MODIS filters used for LAI (single hashed area; Shabanov et al., 2005). Both sets of filter are compared to the laboratory-based spectral reflectance of a maple leaf (*Acer* sp.; Clark et al., 1993). The steep increase in reflectance between the optical and near infrared domains, known as the red-edge, arises from strong chlorophyll absorption at 690 nm and high reflectance by leaf mesophyll cells at 750 nm.

to produce a global product of seasonal (monthly) V_{cmax}^{25} for use in land-surface, carbon and climate models. However, the current study focusses on presenting and validating the methodology for the well-studied sites that constitute FLUXNET. The specific objectives are:

1. To pioneer a new method of retrieving Rubisco-limited photosynthetic capacity from remote sensing and to quantify uncertainties in the technique using a Monte Carlo analysis. Major sources of error are to be identified for future improvement of the methodology.
2. To retrieve seasonal (monthly) Rubisco-limited photosynthetic capacity for several hundred global FLUXNET sites, encompassing 8 PFTs, and make it available to carbon modellers and FLUXNET workers as an online catalogue.
3. For major PFTs, to define and to analyse the range of Rubisco-limited photosynthetic capacity throughout the year. Seasonal measurements have been carried out for individual non-tropical forests and a few crop sites but they lack the multiple-PFT scope and sample sizes of the current study.
4. To determine from the retrieval the spatial variability in Rubisco-limited photosynthetic capacity for sites of the same PFT and to compare this range to compilations of field-based leaf measurements.
5. To quantify and to compare the impacts of spatial and temporal variability on carbon modelling by simulating GPP using a site-specific, time-varying Rubisco-limited photosynthetic capacity, as opposed to the conventional approach of adopting time-constant values per PFT.

2. Material and methods

The methodology is introduced below in the following sequence:

- The conceptual background for the retrieval (Section 2.1);
- The input datasets (Section 2.2);
- The protocol for retrieval at FLUXNET sites (Section 2.3);
- The determination of retrieval uncertainties using a Monte Carlo analysis (Section 2.4);
- The impact on carbon modelling (Section 2.5).

2.1. Conceptual background

The retrieval combines the following 4 steps, the empirical and mathematical basis of which is detailed in Appendix A:

1. Measurements suggest a linear relationship between maximum electron transport for the light reaction ($J_{\max}^{25}$) and leaf chlorophyll content.
2. The sum of leaf chlorophyll content, integrated over canopy LAI, is detected by the hyperspectral index MTCI which has recently been calibrated against ground measurements of chlorophyll (Dash et al., 2010; Vuolo et al., 2012).
3. A fairly tight quasi-linear empirical relationship is observed between $J_{\max}^{25}$ and V_{cmax}^{25}, consistent with the optimisation of active leaf N over a diverse range of C3 plants (e.g. Wullschleger, 1993; Meir et al., 2002; Kattge et al., 2009; Walker et al., 2014).
4. Thus, the chlorophyll concentration per unit ground, derived from remote sensing (step 2 above) can be related to Rubisco-limited photosynthetic capacity summed vertically over the canopy. Equivalently, using the observed exponential vertical decline in active leaf N (Carswell et al., 2000; Lewis et al., 2000; Meir et al., 2002), we can retrieve V_{cmax}^{25} at the canopy top ($V_{cmax}^{25,toc}$) from known values of MTCI and canopy LAI.

The above 4 steps (see Appendix A) yield:

$$240 \times (0.616 \times MTCI - 0.700) = \int_0^{LAI} 428 \left[1 - (24/428) - \exp\left(\frac{-V_{cmax}^{25,toc} \exp(-0.15L)}{158}\right)\right] dL \quad (2)$$

where L is the cumulative LAI from the canopy top to a depth into the canopy. It is the parameter $V_{cmax}^{25,toc}$, on the right side of Eq. (2), which is required for parameterisation of ecophysiological LSMs. The empirical relations adopted in the 4 steps above in order to derive Eq. (2) contain a number of uncertainties which are quantified in Appendix A and accounted for in the Monte Carlo uncertainty analysis below (Section 2.4).

Currently, our retrieval can only be applied to PFTs of type C3 because the relationship $J_{\max}^{25} - V_{cmax}^{25}$ is undocumented for C4 vegetation. Owing to the double exponential on the right side of Eq. (2), $V_{cmax}^{25,toc}$ is solved by forward-modelling. Thus, prior to retrieval, we create a look-up table for the right side of Eq. (2) for narrowly separated values of LAI (ΔLAI = 0.01 m^2 m^{-2}) and $V_{cmax}^{25,toc}$ ($\Delta V_{cmax}^{25,toc}$ = 1 μmol m^{-2} s^{-1}). At each site, observed monthly MTCI is substituted into the left of Eq. (2) and the resulting value is matched against integrals in the look-up table which correspond to the LAI for that month. This yields $V_{cmax}^{25,toc}$. A schematic overview of the methodology is provided in Fig. 2.

2.2. Input datasets for retrieval

2.2.1. Site selection

We use FLUXNET locations which are well studied in terms of vegetation classification, *in situ* LAI and carbon modelling. This selection is consistent with the goal of producing a monthly $V_{cmax}^{25,toc}$ catalogue to improve the parameterisation of carbon models tested against eddy covariance fluxes (Falge et al., 2002). The FLUXNET ancillary database (Agarwal, 2012) provides a list of 376 worldwide sites for which vegetation fits into 8 PFTs of C3 type which are typically used in global LSMs. The distribution of 296 sites, where retrieval is possible (see below), is shown in Fig. 3. Sample sizes and average climate are given in Table 2.

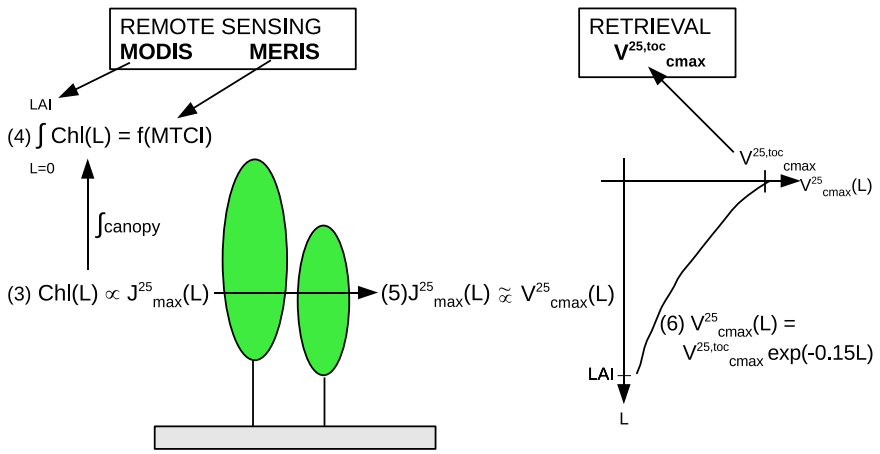

Fig. 2. Schematic overview of the retrieval method. Inputs and outputs are shown in bold. Arrows indicate the connections between the various equations which are enumerated according to Appendix A.

Table 2
Sample sizes and designations for Plant Functional Types (PFTs). The corresponding abbreviation for PFT (Desig.) is adopted in subsequent figures. The number of sites available for retrieval and for carbon modelling are given by n_{site} and n_{siteC}, respectively. The mean and standard deviation (SD) for latitude, Mean Annual Temperature (MAT) and Mean Annual Precipitation (MAP) are given for the carbon modelling sites. Where the number of sites available for carbon modelling is less than 3, only the mean is shown.

PFTs	Desig.	n_{site}	n_{siteC}	Mean ± SD		
				Latitude [°]	MAT [°C]	MAP [mm yr^{-1}]
Non-tropical Broadleaf Forest	BL	67	16	45 ± 6	9 ± 3	946 ± 320
Needleleaf Forest	NL	64	25	47 ± 9	6 ± 6	833 ± 429
C3 crop	Cr3	49	8	42 ± 3	9 ± 3	843 ± 294
Tundra Shrub	Tu	6	1	70	−9	238
Mixed Forest	MX	21	5	43 ± 5	9 ± 4	910 ± 218
Tropical Broadleaf Forest	TBL	25	5	−1 ± 6	25 ± 0	2433 ± 651
C3 grass	C3	52	11	37 ± 4	13 ± 3	694 ± 384
Non-tundra Shrub	SH	12	2	37	11	404

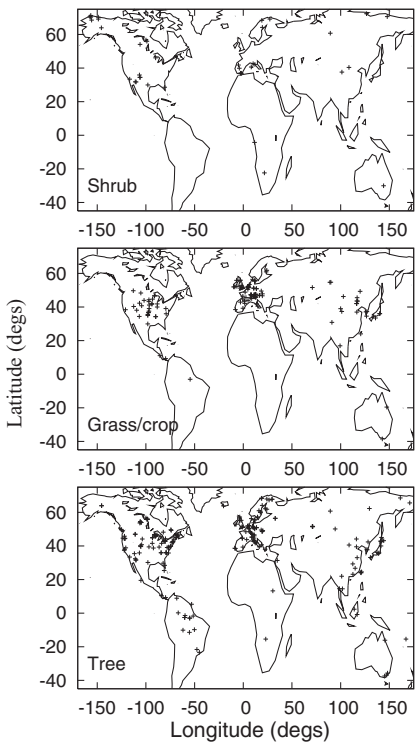

Fig. 3. The distribution of FLUXNET locations used for the retrieval of $V_{cmax}^{25,toc}$. For clarity, a coarse categorisation based on life form (tree, grass/crop and shrub) is depicted but sites are partitioned into 8 PFTs within the study.

2.2.2. MTCI from MERIS

We access the standard MTCI product (Curran et al., 2007) from the NERC Earth Observation Data Centre (NEODC) which provides monthly values at a spatial resolution of 0.04° for the global ice-free land-surface over a 9 yr MERIS operational period (2003–2011). Pixels are mean-averaged to 0.12° to provide a footprint (9 km at a typical site latitude of 45°) comparable to the input LAI from MODIS (discussed below).

Note that the LAI retrieved by MODIS and other satellite detectors (e.g. AVHRR and SPOT) is based on broadband optical and near-infrared reflectance rather than the narrowband filters used by MTCI to quantify the gradient in the red-edge (Fig. 1). The two sets of filters (MERIS and MODIS) are independent, although the inference of both chlorophyll concentration and LAI relies on the relatively high reflectance in the near-infrared compared to the optical domain. Note that the MTCI derived from laboratory spectra of broad and needle leaves correlates strongly with measured chlorophyll content (R^2 = 0.6–0.8; Dash and Curran, 2007). Further, for cereal crops and grassland sampled within the MERIS footprint, the chlorophyll concentration per unit ground correlates very strongly (R^2 = 0.80) with MTCI (Dash et al., 2010).

2.2.3. LAI from MODIS

To create an LAI timeseries for 2003–2011, we extract from the 8-day MOD15A2 (C5) LAI product a 7 km × 7 km subset (49 pixels) centred on the site. Note that smaller subsets are considered less robust in terms of the LAI produced by the MODIS radiative-transfer algorithm (Yang et al., 2006a,b; Heinsch et al., 2006). We mean average pixels of good quality (i.e. main algorithm, no

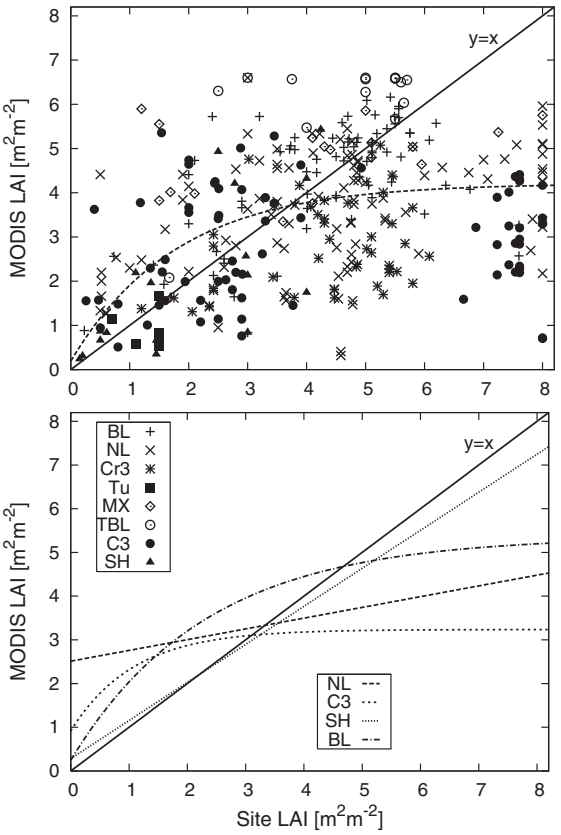

Fig. 4. Maximum field-recorded site Leaf Area Index (LAI) plotted against the corresponding satellite (MODIS) measurement. In the upper panel, each marker corresponds to a siteyear for which site LAI is available during the growing season. Marker type corresponds to PFT, which is abbreviated according to Table 2. Measurements in the upper panel are used to derive least-square empirical fits between MODIS and site data for each PFT. The lower panel shows these empirical fits for PFTs with the smallest (non-tropical broadleaf forest and non-tundra shrub) and largest (C3 grass and needleleaf forest) root-mean-square difference between site and MODIS observations (excluding tundra shrub for which the empirical fit is poorly defined). In the upper panel, the dashed line corresponds to the best fit for all PFTs combined. See Table 3 for empirical fits for all PFTs.

significant cloud and >50% detectors working; Yang et al., 2006b). To minimise noise in the phenology timeseries (De Kauwe et al., 2011), the spatial mean is averaged temporally using a median 32-day moving window, except for the tropics where persistent cloud (Zhao et al., 2005) necessitates selection of the maximum LAI value over a moving 48-day window (Ryu et al., 2011).

Note that a field-based timeseries of LAI does not exist at most FLUXNET sites (Melaas et al., 2013). Therefore, only MODIS provides the sampling necessary to retrieve photosynthetic capacity across the seasonal cycle. However, we normalise the MODIS timeseries to the site LAI recorded during the peak growing season. Thus, for each year, maximum site LAI is selected from the FLUXNET ancillary archive (Agarwal, 2012) and the MODIS timeseries for that year is normalised so that site measurement and MODIS agree for the day on which site LAI is measured. We do not use site LAI based on leaf fall since detailed knowledge of senescence and leaf-out is required to reconstitute canopy LAI in this case. When the site LAI is unavailable, we substitute a PFT-specific empirical relation developed in Table 3 between site and MODIS LAI.

Since LAI is an important input to the retrieval, we summarise discrepancies between site and MODIS LAI evident in the above normalisation. Overall, there is a tendency for the satellite to underestimate field-based measurements when LAI is high and to overestimate field-based measurements when field LAI is low (Fig. 4). At high LAI, canopy reflectance saturates and the MODIS calibration still needs to be improved to take account of this (De Kauwe et al., 2011; Fang et al., 2012; Serbin et al., 2013). The satellite may overestimate low field-based LAI since the latter typically misses below-canopy vegetation (e.g. the herbal layer). However, in several cases where field-based LAI is low, the site is recovering from disturbance (e.g. clear-felling or burning; Law et al., 2002) and is, therefore, unrepresentative of the satellite footprint. This is corroborated by MERIS which often indicates high chlorophyll levels across the MODIS footprint. Thus both satellite inputs (LAI and MTCI) are consistent with vegetation which is denser than that recorded *in situ*. In this case, a calibration of input LAI timeseries to low site LAI can yield spuriously high values of $V_{cmax}^{25,toc}$ since LAI appears in the denominator in the retrieval (crudely, $V_{cmax}^{25,toc} \sim$MTCI/f(LAI)). Furthermore, for thin or sparse vegetation cover (LAI <1.5 $m^2\ m^{-2}$), there is a heightened sensitivity to background (soil) reflectance making the retrieved $V_{cmax}^{25,toc}$ highly uncertain. To mitigate these two problems, the retrieval is only undertaken when monthly LAI $\geq$1.5 $m^2\ m^{-2}$. This removes a large percentage (36%) of the 45,000 potential monthly retrievals but it does allow $V_{cmax}^{25,toc}$ to be retrieved across the growing season for the majority of sites. For LAI $\geq$1.5 $m^2\ m^{-2}$, more than half the downwelling shortwave radiation is incident on leaves rather than the ground, assuming a turbid leaf canopy with a spherical leaf angular distribution (Campbell and Norman, 1998, p. 249).

Our main retrieval, referred to as "site-norm", uses the site-normalised LAI. However, to gauge sensitivity to input LAI and a potential mismatch between satellite and site footprints, we undertake a second retrieval, referred to as "sat-only", which omits the normalisation of the MODIS timeseries to site LAI. For this second retrieval, the filter LAI $\geq$1.5 $m^2\ m^{-2}$ is still applied in order to reduce sensitivity to soil background.

2.3. Protocol for implementation at FLUXNET sites

For each FLUXNET location, a monthly MTCI timeseries for 2003–2011 is created using the 0.12° pixel containing the latitude and longitude of the site. From the corresponding 8-day LAI timeseries, created for each site, LAI is extracted for the month in question via bilinear interpolation of the two acquisitions straddling the middle of the month. $V_{cmax}^{25,toc}$ is retrieved from the look-up table created for Eq. (2), using observed values of MTCI and LAI. This is done for each month of the period 2003–2011 for each site. The retrieval is carried out three times, using: (1) the site-normalised LAI timeseries (site-norm); (2) an unnormalised LAI timeseries (sat-only); and (3) as site-norm but using an alternative MTCI-calibration (site-norm-cal2) based on a different landcover (Vuolo et al., 2012); see Appendix A).

Retrieved values of $V_{cmax}^{25,toc}$ are compared with field observations at several different levels of aggregation:

1. We create the average seasonal cycle per site ($V_{cmax}^{25,toc}(site, month)$) by median averaging values for the same month over the retrieval period 2003-2011. Median averaging reduces random noise associated with input LAI, which, on occasion, can be quite large (De Kauwe et al., 2011). $V_{cmax}^{25,toc}(site, month)$ is made available as an online catalogue which can be compared with field measurements at individual locations e.g. Walker Branch broadleaf forest (Wilson et al., 2000).
2. For each site, the 3 highest values of $V_{cmax}^{25,toc}(site, month)$ from across the year are extracted (corresponding to peak growing season) and are pooled according to PFT in order to compare the frequency distribution against compilations of field observations (Wullschleger, 1993; Kattge et al., 2009; Wright et al., 2005; Beerling and Quick, 1995).

Table 3
Optimised parameters for a least-squares empirical fit between ground-based (site) LAI and satellite (MODIS) LAI. The fit is conducted separately for each Plant Functional Type (PFT) by pooling all relevant siteyears where site LAI is available (sample size *n*). Optimised fitting parameters (a, b and c) correspond to the simplest functional form which fits the data satisfactorily. Where *a*, *b* and *c* are all given, the fitted function takes the form $y = a - c \times exp(-x/b)$ where *x* and *y* denote site and MODIS LAI, respectively. Where only *a* and *b* are given, $y = ax + b$. For tundra shrub, $y = ax$. RMS(*y*-MODIS) is the root-mean-square difference between the best fit and MODIS LAI, expressed in absolute terms ($m^2 m^{-2}$) and as a percentage of mean MODIS LAI. RMS(MODIS-site) is the root-mean-square difference between the site and MODIS observations, expressed as $m^2 m^{-2}$ and as a percentage of mean site LAI. See Fig. 4 for a graphical presentation.

PFT	a	b	c	RMS [$m^2 m^{-2}$ (%)]		*n*
				(*y*-MODIS)	(MODIS-site)	
Non-tropical Broadleaf Forest	5.36	2.32	5.11	1.00 (22)	1.32 (30)	78
Needleleaf Forest	0.25	2.51	–	1.22 (34)	2.16 (48)	99
C3 crop	3.10	1.12	6.48	0.89 (32)	2.13 (49)	45
Tundra Shrub	0.65	–	–	0.47 (52)	0.67 (51)	6
Mixed Forest	0.13	4.30	–	0.72 (14)	1.98 (47)	17
Tropical Broadleaf Forest	0.54	3.59	–	0.89(14)	1.82 (39)	15
C3 grass	3.24	1.08	2.32	1.22 (43)	3.02 (73)	72
Non-tundra Shrub	0.87	0.28	–	1.17 (58)	1.18 (59)	17

3. For sites within the same PFT, we median average $V_{cmax}^{25,toc}(site, month)$ from (1) above to produce an average seasonal cycle per PFT ($V_{cmax}^{25,toc}(pft, month)$).

2.4. Monte Carlo uncertainty analysis

The retrievals site-norm and sat-only take some account of systematic errors in LAI. However, there are also systematic errors in the adopted empirical biochemical relations yielding Eq. (2) as well as random measurement errors in both LAI and MTCI. The impact of these errors is estimated using a Monte Carlo analysis. Thus, to quantify our uncertainty in $V_{cmax}^{25,toc}$, we assume the following errors and propagate them in the retrieval method:

1. 0.2 in MTCI owing to soil background variation (Vina et al., 2011), which is applied randomly, but time-invariantly, to each site;
2. 10% in LAI which is random for each monthly timestep (typical, although larger random errors occur sporadically with MODIS; De Kauwe et al., 2011);
3. a 12% error in the empirical parameter a_{wull}, which relates $J_{\max}^{25}$ to V_{cmax}^{25} (Eq. (5) in Appendix A) owing to best-fit differences across different databases (Wullschleger, 1993; Kattge et al., 2009; Walker et al., 2014). The error is applied randomly in Eq. (5) (Appendix A) and propagated to Eq. (2) before beginning the retrieval process (thus applied to all sites and timesteps);
4. a 16 $\mu mol\, m^{-2}\, s^{-1}$ systematic error in the empirical parameter b_{chl} which relates leaf chlorophyll content to $J_{\max}^{25}$ (equivalent to 13% mean $J_{\max}^{25}$). The error is applied randomly in Eq. (3) (Appendix A) and propagated to Eq. (2) before beginning the retrieval process (thus applied to all sites and timesteps).

Random selection is from a Gaussian (normal) probability distribution, with standard deviation set to the errors specified above, prior to the retrieval. The standard deviation in the retrieval, over 500 realisations of these error selections, indicates the uncertainty in $V_{cmax}^{25,toc}$. Uncertainties are propagated to the seasonal cycles at site and PFT levels (aggregation steps (1)–(3) in Section 2.3). Although the number of realisations is limited by computer time, the standard deviation converges sufficiently well to quantify the uncertainties with adequate precision.

2.5. Impact on carbon modelling

For a subset of our sites ($n = 73$; Table 2) where tower meteorology is freely available to the general modelling community (www.fluxnet.org), we force a state-of-the-art LSM with retrieved monthly $V_{cmax}^{25,toc}$ from the main retrieval and compare output GPP with that from a traditional or conventional carbon simulation. Three experiments are organised as follows:

1. A novel simulation using $V_{cmax}^{25,toc}(site, month)$ which accounts for both temporal (seasonal) and spatial (sub-PFT) variability in Rubisco-limited photosynthetic capacity.
2. A conventional simulation, similar to that adopted by most global LSMs, which takes no account of either temporal or sub-PFT spatial variability. In this case, $V_{cmax}^{25,toc}$ is time-invariant and is assigned the median value from the growing seasonal retrievals for the PFT in question (available via step (2) of the protocol in Section 2.3).
3. A novel simulation using the PFT average seasonal cycle, $V_{cmax}^{25,toc}(pft, month)$, as derived in step (3) of the protocol above (Section 2.3). This experiment accounts for temporal, but not sub-PFT (spatial), variability.

Note that, for experiments (1) and (3) above, bi-linear interpolation is used to fill out months where values are missing (typically, outside of the growing season when LAI <1.5 $m^2\, m^{-2}$).

The LSM adopted in the experiments is an ecophysiological process-based model called JULES-SF (Joint UK Land Environmental Simulator). It uses a Farquhar-type biochemical co-limitation photosynthetic submodel based on V_{cmax}^{25} (Collatz et al., 1991) which is linked to a Ball-Berry stomatal submodel (Ball et al., 1987; Collatz et al., 1991). Leaf photosynthesis is calculated at different heights within the canopy before being summed to produce ecosystem GPP. JULES-SF is one of most elaborate LSMs which operates globally in terms of light interception, by taking account of direct and diffuse sunlight at different depths within the canopy (Alton et al., 2007). Within the model, photosynthetic capacity declines exponentially from the canopy top downwards in a manner consistent with both field observations (Carswell et al., 2000; Lewis et al., 2000; Meir et al., 2002) and the assumptions of the retrieval (Appendix A). Canopy temperature for photosynthesis is derived from the Penman-Monteith energy balance (Monteith, 1965).

In addition to $V_{cmax}^{25,toc}$, JULES-SF requires a number of (typically PFT-dependent) biophysical parameters, which are prescribed according to average collated field measurements available within the literature (Alton and Bodin, 2010). To prescribe site-specific soil hydraulic properties, we adopt the average soil composition measured at each site in the FLUXNET ancillary database (Agarwal, 2012) and relate the recorded clay and silt to the categorisation of soil properties given in Campbell and Norman (1998).

For all 3 experiments above, the model is forced by tower meteorology (averaged to a 3-h timestep) and the site-normalised 8-day MODIS LAI timeseries. In order to produce a smooth output for GPP, both input LAI and $V_{cmax}^{25,toc}$ are interpolated to the 3-h

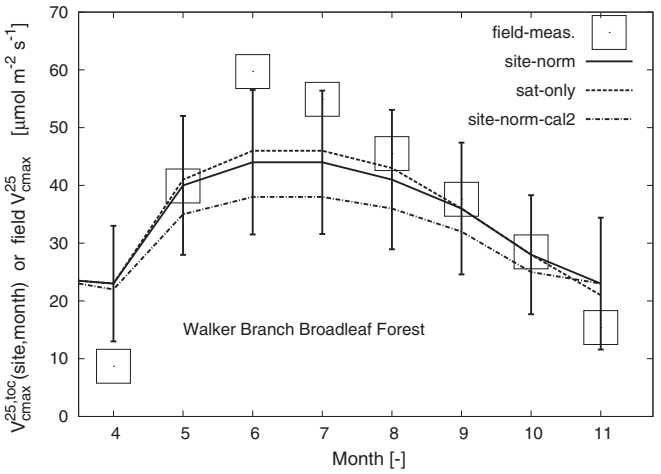

Fig. 5. Monthly top-of-canopy Rubisco-limited photosynthetic capacity ($V_{cmax}^{25,toc}$(*site*, *month*)) retrieved for the non-tropical broadleaf forest at Walker Branch compared with *in situ* leaf measurements of V_{cmax}^{25} (growing season capacity near, but not at, the canopy top) collected by Wilson et al. (2000). The field measurements are averaged over two seasons using a monthly timestep and the markers (squares) correspond in size to the standard error. The three retrievals are shown: normalisation to site LAI (site-norm); unnormalised LAI (sat-only) and normalised LAI with alternative MTCI-calibration (site-norm-cal2). Uncertainties for the main retrieval (site-norm) are derived from the Monte Carlo analysis and are represented by errorbars.

internal timestep of the model. Since the $V_{cmax}^{25,toc}$ forcing is the median average over the MERIS operating period (2003–2011), the same photosynthetic capacity forcing is used for different years at the same site.

Simulations for each site are run separately for each year. Where the siteyear meteorology precedes the available MODIS timeseries (<2003), a median MODIS LAI timeseries is used, averaging years 2003–2011 and normalised to site LAI. Although the tower meteorology is usually complete over the growing season, protracted gaps can exist during winter for some siteyears owing to instrument failure (Falge et al., 2002). In order to be able to produce GPP for the whole year, these gaps are filled with the Princeton 3-h reanalysis meteorology (Sheffield et al., 2006) using the 1° grid square corresponding to the longitude and latitude of the site. Soil moisture content for each siteyear is spun-up by splicing the corresponding meteorology and phenology back-to-back over a 5 yr period and pre-running the model over this period.

3. Results and discussion

3.1. Individual locations and site catalogue

Fig. 5 shows the average seasonal cycle of Rubisco-limited photosynthetic capacity retrieved for Walker Branch forest ("non-tropical broadleaf forest" in our PFT classification) against average *in situ* leaf measurements (Wilson et al., 2000). We have median averaged monthly retrievals across all MERIS years (2003–2011), producing $V_{cmax}^{25,toc}$(*site*, *month*), in order to reduce noise and also because the field measurements predate the retrieval period. The field measurements are for sunlit foliage near the canopy top (therefore, strictly V_{cmax}^{25} rather than $V_{cmax}^{25,toc}$) and vary somewhat between years, especially in late summer when drought may occur. However, such variation (±5 μmol m^{-2} s^{-1}) is sufficiently small to make the comparison between $V_{cmax}^{25,toc}$(*site*, *month*) and average field measurements a valid test of the retrieval method.

$V_{cmax}^{25,toc}$(*site*, *month*) is seasonally variant (though less so than the field observations). Therefore, implementation of a time-invariant Rubisco-limited photosynthetic capacity within LSM calculations of annual photosynthesis (e.g. Medlyn et al., 2005; Kattge et al., 2009) is likely to lead to errors (see discussion below in Section 3.4). Despite large uncertainties in our methodology, the retrieval is similar in magnitude to *in situ* field measurements but falls short of the peak field values in June and July. This is true of all 3 retrievals (site-norm, sat-only, site-norm-cal2), suggesting that uncertainties in the LAI and MTCI calibrations cannot explain the discrepancy between the retrieval and field measurements. In contrast, the uncertainties indicated by the Monte-Carlo analysis, represented by error bars in Fig. 5, are much larger. They are dominated by systematic uncertainties in the empirical biochemical relations $J_{\max}^{25}$-V_{cmax}^{25} and $J_{\max}^{25} - Chl$ (Section 2.4).

Field observations at Walker Branch reveal a spring peak and a gentle decline through the summer. A similar behaviour is also recorded in leaf measurements at other non-tropical broadleaf forests (Xu and Baldocchi, 2003; Grassi et al., 2005). In contrast, retrieved values vary much less over the season owing to the shallow gradient of the adopted $J_{\max}^{25} - Chl$ relation and, ultimately therefore, a fairly low sensitivity of $V_{cmax}^{25,toc}$ to variation in MTCI. Thus, retrieved values vary by a factor of 2 across the season at Walker Branch, whilst field measurements indicate a change of factor 5.

Wilson et al. (2000) raise the concern that the impact of drought is omitted in LSMs owing to use of constant V_{cmax}^{25}. However, this is a misconception of how LSMs operate. LSMs adopting a Farquhar co-limitation calculation of photosynthesis, such as JULES-SF, CLM (Bonan et al., 2011) and SiB (Sellers et al., 1996), usually assume that V_{cmax}^{25} is a purely physiological property of the leaf, proportional to foliar Rubisco content. Thus, whilst V_{cmax}^{25} remains constant, such models reduce leaf photosynthetic rate according to stress factors for temperature and soil moisture (e.g. Eq. (C17) of Sellers et al., 1996), and a leaf stomatal conductance which is sensitive to atmospheric humidity (e.g. Collatz et al., 1991). V_{cmax}^{25} inferred from leaf-level measurements (A-c_i empirical relationship) assumes drought-free plants but such conditions seldom prevail throughout the entire growing season. To infer the true underlying V_{cmax}^{25} from A_{max} measured in the field, a stress factor for soil moisture should be added to the Farquhar relation used in the inference method (e.g. to the right side of Eq. (1) in Wullschleger, 1993). In the absence of this stress factor, the seasonal amplitude of the leaf measurements could be exaggerated.

We follow the same procedure as Walker Branch in Fig. 5 and produce an average seasonal cycle ($V_{cmax}^{25,toc}$(*site*, *month*)) for all 296 sites in our sample where a retrieval is possible. This catalogue is made freely available online (Appendix B) and is intended for comparison with field measurements or for forcing of carbon models.

3.2. Growing season values (PFT evaluation)

For each site belonging to a given PFT, we extract and pool the 3 highest values from the average seasonal cycle $V_{cmax}^{25,toc}$(*site*, *month*) and determine the median and interquartile range from the pool for each PFT. The objective is to compare with compilations of field observations typically undertaken during the peak of the growing season. The median and the interquartile range, rather than the mean and the standard deviation, are evaluated where possible in order to reduce the impact of outliers and a skewed frequency distribution (see below).

Fig. 6 compares retrieved values with compilations of field-based values inferred either from fitting a Farquhar-type empirical model to maximum recorded leaf photosynthesis, A_{max} (Wullschleger, 1993; Kattge et al., 2009; Wright et al., 2005) or from isotope δ^{13}C analysis (Beerling and Quick, 1995). Note that, for all compilations of field observations, V_{cmax}^{25} is not measured directly but is inferred. For the field compilation of Wright et al. (2005)

Table 4
Average and range for retrieved and field-based maximum carboxylation rate or Rubisco-limited photosynthetic capacity (μmol m^{-2} s^{-1}), shown per PFT. On the left side, we show the median, interquartile range (IQR25 and IQR75) and sample size (n) of retrieved $V_{cmax}^{25,toc}(site, month)$ for the peak growing season. These quantities are shown for the main (site-norm), unnormalised-LAI (sat-only) and alternative MTCI-calibration (site-norm-cal2) retrievals. The right side summarises field-based compilations of V_{cmax}^{25} (growing season photosynthetic capacity but not necessarily at canopy top). The median, interquartile range and sample size are shown for Wright et al. (2005). Mean ± SD (n), where SD is the standard deviation, is shown for Kattge et al. (2009) and Wullschleger (1993). A single field-based estimate, using isotopes, is also given (BQ; Beerling and Quick, 1995). The mean average of the field-based compilations (Wright et al.; Kattge et al.; Wullschleger; and Beerling & Quick) is shown in the column <Field>.

PFT	Retrieved $V_{cmax}^{25,toc}(site, month)$				Field-based V_{cmax}^{25}			
	Median$\pm^{IQR75}_{IQR25}(n)$			Median$\pm^{IQR75}_{IQR25}(n)$	Mean$\pm SD(n)$			
	Sat-only	Site-norm	Site-norm-cal2	Wright et al.	Kattge et al.	Wullschleger	BQ	<Field>
Non-tropical Broadleaf Forest	$46\pm^{8}_{7}$ (245)	$46\pm^{8}_{5}$ (202)	$39\pm^{5}_{3}$ (202)	$40\pm^{12}_{9}$ (186)	58 ± 21 (404)	47 ± 33 (19)	36	45
Needleleaf Forest	$44\pm^{7}_{12}$ (202)	$39\pm^{7}_{8}$ (191)	$34\pm^{6}_{5}$ (191)	$29\pm^{10}_{3}$ (24)	63 ± 25 (220)	25 ± 12 (10)	42	39
C3 crop	$57\pm^{13}_{10}$ (151)	$45\pm^{13}_{6}$ (147)	$39\pm^{10}_{5}$ (147)	–	101 ± 37 (209)	88 ± 38 (158)	122	103
Tundra Shrub	$31\pm^{3}_{12}$ (20)	$23\pm^{5}_{6}$ (18)	$22\pm^{4}_{5}$ (18)	$45\pm^{16}_{12}$ (11)	–	–	22	33
Mixed Forest	$45\pm^{5}_{5}$ (72)	$43\pm^{5}_{4}$ (63)	$37\pm^{3}_{3}$ (63)	–	–	–	50	50
Tropical Broadleaf Forest	$46\pm^{3}_{4}$ (78)	$52\pm^{3}_{5}$ (75)	$44\pm^{2}_{4}$ (75)	$36\pm^{9}_{14}$ (105)	41 ± 15 (107)	51 ± 31 (22)	78	51
C3 grass	$47\pm^{6}_{8}$ (184)	$42\pm^{11}_{7}$ (154)	$37\pm^{7}_{6}$ (154)	$54\pm^{16}_{14}$ (21)	78 ± 31 (254)	66 ± 49 (10)	44	60
Non-tundra Shrub	$39\pm^{13}_{10}$ (40)	$43\pm^{10}_{6}$ (34)	$37\pm^{7}_{5}$ (34)	$45\pm^{15}_{10}$ (112)	58 ± 20 (282)	53 ± 15 (7)	–	52

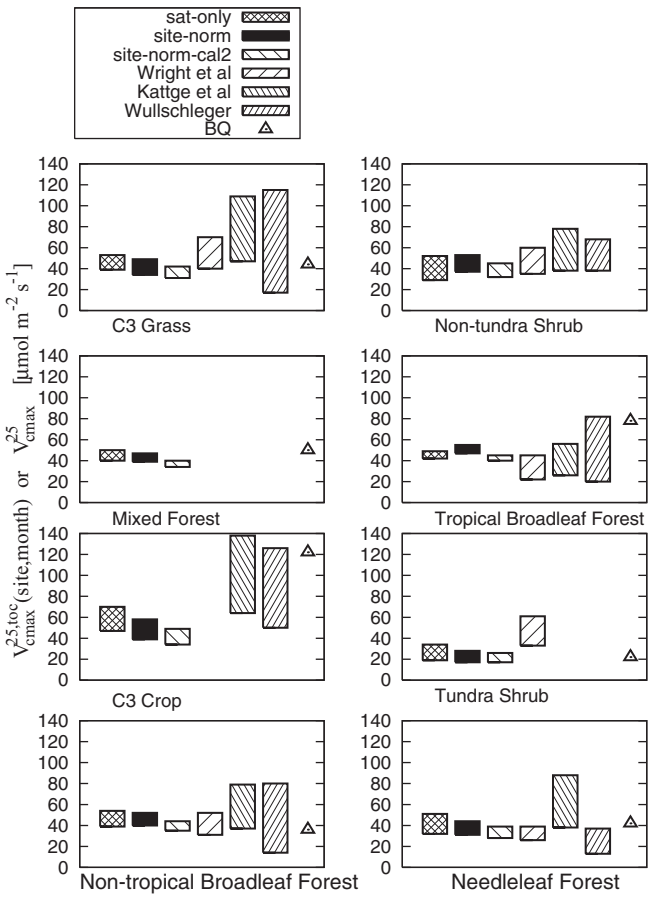

Fig. 6. Barcharts comparing the range of retrieved $V_{cmax}^{25,toc}(site, month)$ against compilations of field-based V_{cmax}^{25} by Kattge et al. (2009), Wright et al. (2005), Wullschleger (1993) and Beerling and Quick, 1995;BQ). Values are grouped according to PFT. BQ is based on a single estimate per PFT. Retrievals are situated on the left of each panel and are denoted by "site-norm", "sat-only" and "site-norm-cal2".

we follow the same procedure as Kattge et al. to infer V_{cmax}^{25} from A_{max}. Our retrieved values generally lie in the middle of the field-based range, with the exception of C3 crops (Table 4). However, retrieved values possess a smaller range than field-based measurements (typically IQR/median ≃ 0.4, where IQR is the interquartile range, compared to 0.6, 0.5 and 0.7 for Wright et al., Kattge et al. and Wullschleger et al., respectively). This is probably due to the shallow gradient of the adopted $J_{\max}^{25} - Chl$ relation. However, the satellite footprint provides an ecosystem average rather than capturing the full range of individual species as in the field observations.

Even with their large ranges, some field observations are mutually exclusive e.g. values for needleleaf forest differ between Wullschleger (1993) and Kattge et al. (2009). For the compilations of Wullschleger (1993), Kattge et al. (2009) and Wright et al. (2005), some disparity in the inferred values probably arises from the precise formulation adopted in the Farquhar model. For example, Wullschleger does not take explicit account of either the temperature or the assimilation compensation point of the leaf. In their method, Beerling and Quick (1995) use maximum leaf photosynthetic rate for individual PFTs and the long-term intercellular CO_2 concentration, c_i, inferred from the leaf isotope ratio $\delta^{13}C$. Excluding C3 crops (discussed separately below), the root-mean-square difference between the PFT-median from the main retrieval (site-norm) and the mean of the field-based averages (columns 3 and 9 in Table 4) is 9.2 μmol m^{-2} s^{-1} (equivalent to ≃18% field-based). This is comparable to the dispersion amongst the field-based averages themselves (12 μmol m^{-2} s^{-1} or 24% of field-based). Thus, in general, our remote sensing method does not yield average values which are systematically different from the field-based estimates.

All 3 retrievals produce similar median values and ranges, particularly when compared against field-based measurements (Fig. 6). Thus, the PFT medians of the sat-only and site-norm retrievals (columns 2 and 3 in Table 4) differ by a root-mean-square difference of 6.5 μmol m^{-2} s^{-1} (sat-only on average 7% higher). Similarly, site-norm and site-norm-cal2 (columns 3 and 4 in Table 4) differ by a root-mean-square-difference of 5.9 μmol m^{-2} s^{-1} (sat-norm-cal2 on average 13% lower). For most PFTs, then, we retrieve a similar range of $V_{cmax}^{25,toc}$, whether the input LAI timeseries is site-normalised or not. For C3 crops, the satellite footprint subtends either heterogeneous vegetation or crops in different growth stages. In particular, many C3 crop sites are surrounded by vegetation of a lower LAI. Since retrieved $V_{cmax}^{25,toc} \sim$ MTCI/f(LAI), substitution of unnormalised (sat-only) LAI increases retrieved values by 27% compared to the main (site-norm) retrieval. Thus, LAI input is a significant source of uncertainty for this PFT and, indeed, comparable with the systematic uncertainty in the retrieved PFT median arising mainly from the adopted biochemical relations (Table 5).

Regardless of whether the input LAI timeseries is site-normalised or not, retrieved values for C3 crops are only about half the value inferred from field measurements (Fig. 6). One potential problem is the use of a general relation for $J_{\max}^{25} - Chl$ which may be inappropriate for some PFTs. Thus, C3 crop, represented by barley, lies 50% above the best linear fit in Fig. 10 ($x = 0.36$, $y = 168$), suggesting that we may significantly underestimate $J_{\max}^{25}$ and hence $V_{cmax}^{25,toc}$

Table 5
Uncertainties in retrieved Rubisco-limited photosynthetic capacity from the main retrieval (site-norm) according to PFT and based on a Monte Carlo propagation of errors. Uncertainties are shown for the median and the 25th (IQR25) and 75th (IQR75) percentile range given in Table 4. The uncertainty is expressed in both absolute (μmol m^{-2} s^{-1}) and percentage terms (latter in parentheses).

PFT	Absolute uncertainty (percentage uncertainty) [μmol m^{-2} s^{-1}] (%)		
	Median	IQR25	IQR75
Non-tropical Broadleaf Forest	11 (24)	10 (26)	12 (23)
Needleleaf Forest	10 (27)	9 (31)	11 (25)
C3 crop	11 (26)	11 (28)	13 (22)
Tundra Shrub	8 (35)	8 (50)	8 (31)
Mixed Forest	11 (26)	10 (28)	11 (25)
Tropical Broadleaf Forest	12 (23)	11 (24)	12 (23)
C3 grass	10 (26)	10 (31)	11 (23)
Non-tundra Shrub	10 (23)	9 (25)	11 (22)

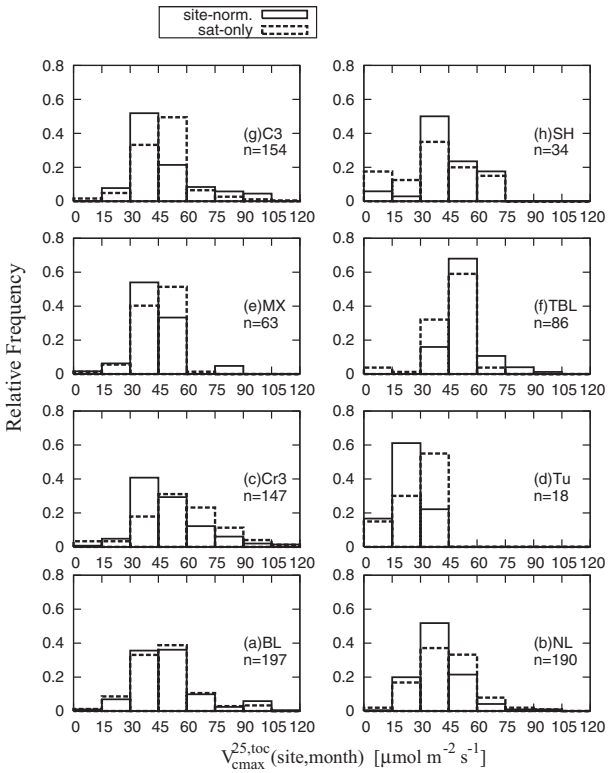

Fig. 7. Relative histogram of $V_{cmax}^{25,toc}(site, month)$ for the peak growing season for sites grouped according to PFT. PFTs are abbreviated according to Table 2. The sample size is *n*. Histograms are shown for the main (site-norm) and unnormalised LAI (sat-only) retrieval.

for this PFT. Clearly, our retrieval would benefit from a larger availability of leaf chlorophyll measurements undertaken for specific vegetation types.

Histograms reveal a distribution of retrieved values which is similar for both site-norm and sat-only (site-norm-cal2 resembles site-norm but is shifted to somewhat smaller $V_{cmax}^{25,toc}$; Fig. 7). Again, the main exception is C3 crops, and perhaps C3 grass, where the distribution is shifted to higher values for unnormalised LAI. Note, that the distribution is poorly defined for some PFTs where sample size is small (e.g. tundra and non-tundra shrub). In general, the histogram distributions are fairly broad, although somewhat less so than field-based measurements (Kattge et al., 2009; Wright et al., 2005). This underlines the crudeness of implementing a single PFT average in LSM global carbon simulations. A long positive tail is noted in field-based compilations especially for C3 crops and grasses, extending up to 200 μmol m^{-2} s^{-1} (Kattge et al., 2009; Wullschleger, 1993).

3.3. Seasonal variation per PFT

The average seasonal cycles $V_{cmax}^{25,toc}(site, month)$ for sites of the same PFT are pooled and values in each month are median-averaged to define an average seasonal cycle for the same vegetation type ($V_{cmax}^{25,toc}(pft, month)$). LAI and MTCI are treated likewise to compare phenological inputs against retrieval output. Except for tropical broadleaf forest, the seasonal cycles of LAI and $V_{cmax}^{25,toc}(pft, month)$ peak in the middle of the year since the majority of the sites are situated in the northern hemisphere (Fig. 3 and Table 2). This geographical bias allows us to create a PFT average cycle.

$V_{cmax}^{25,toc}(pft, month)$ changes considerably throughout the year for all PFTs except tropical broadleaf forest (Fig. 8). Dividing the maximum retrieved value across the seasonal cycle by the minimum value, yields a typical temporal variation of factor 1.6. Even for needleleaf forest, which consists mostly of evergreen foliage, there is a seasonal cycle in retrieved $V_{cmax}^{25,toc}(pft, month)$. Field measurements of needleleaves corroborate a seasonal variation (Dang et al., 1998; Ellsworth, 2000; Misson et al., 2006; Han et al., 2008), although it is generally less pronounced than that of non-tropical broadleaf trees (Xu and Baldocchi, 2003; Grassi et al., 2005).

Even for non-tropical PFTs, $V_{cmax}^{25,toc}(pft, month)$ usually remains quite high during the northern hemisphere winter. The prerequisite for retrieval (LAI≥1.5 m^2 m^{-2}; Section 2.2.3) ensures that only sites with some green vegetation contribute to this "dormant" period. Furthermore, we are averaging over sites whose peak growth may occur at different times of the year (e.g. winter crops, bi-annual greening at mediterranean sites) which convolutes the general seasonal cycle. Our sample sizes preclude a narrower geographic segregation of the data. Indeed, the seasonal profiles for both tundra and non-tundra shrub in Fig. 8 are quite uncertain owing to small sample sizes ($n = 6$ for July and $n = 1$–3 for winter months).

3.4. Impact on carbon modelling

Fig. 9 demonstrates the impact of forcing the land-surface model JULES-SF with a temporally and spatially variable Rubisco-limited photosynthetic capacity by comparing against a conventional simulation which uses a Rubisco-limited photosynthetic capacity which is both time-invariant and fixed per PFT. Panel (a) of Fig. 9 reveals two effects (temporal and spatial) which are better isolated in panels (b) and (c).

Firstly, GPP is reduced by 11% owing to the time-varying forcing of $V_{cmax}^{25,toc}$. This assertion is based on averaging across all sites except tropical broadleaf forest (for which Rubisco-limited photosynthetic capacity is seasonally fairly constant). A reduction in simulated GPP can be expected given that the value adopted for constant $V_{cmax}^{25,toc}$ is taken from the median retrieval in Table 4, which is based on the highest values retrieved across the growing season. For most FLUXNET sites, the decrease in $V_{cmax}^{25,toc}(site, month)$

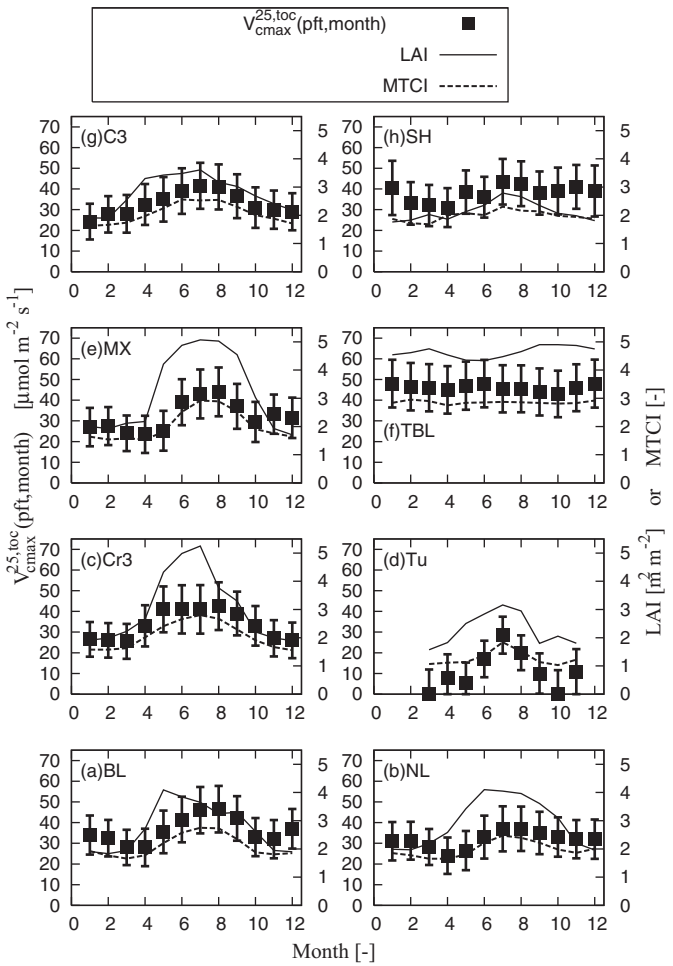

Fig. 8. The PFT average seasonal cycle of retrieved Rubisco-limited photosynthetic capacity, $V_{cmax}^{25,toc}(pft, month)$ (left axis), compared to the corresponding average inputs of LAI and MTCI (right axis). PFTs are abbreviated according to Table 2.

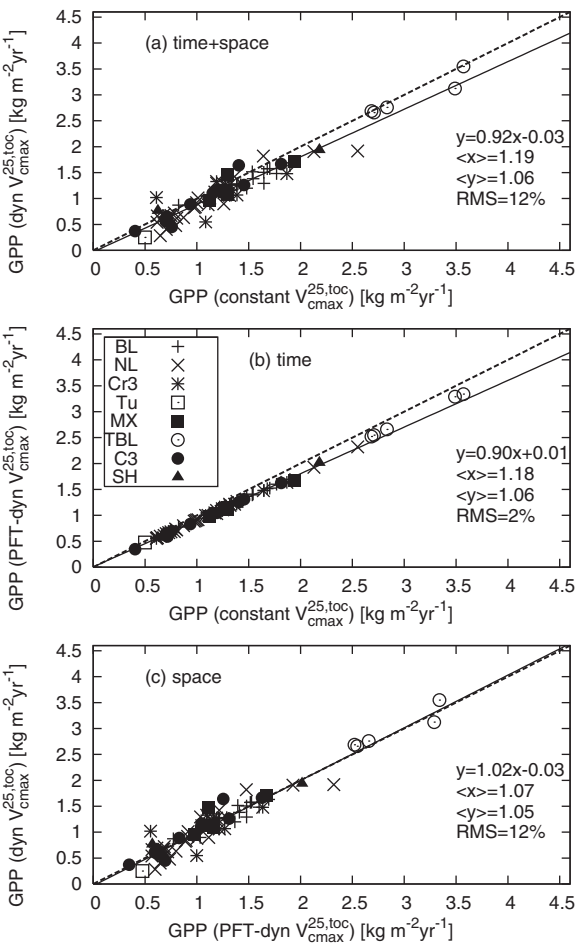

Fig. 9. Simulated annual Gross Primary Product (GPP) with time-varying, site-specific forcing in Rubisco-limited photosynthetic capacity, $V_{cmax}^{25,toc}(site, month)$ (denoted "dyn"), compared against a conventional simulation of time-invariant Rubisco-limited photosynthetic capacity per PFT (denoted "constant"). To isolate the temporal and spatial effects (panels b and c, respectively), the model is also forced with the PFT average seasonal cycle, $V_{cmax}^{25,toc}(pft, month)$, which is denoted by "PFT-dyn". Each marker denotes a different site (averaged across all available siteyears) and each marker-type denotes a different PFT (abbreviated according to Table 2). Average variates are given by <x> and <y>. The least-squares linear fit (excluding tropical broadleaf forest) and $y = x$ are represented by solid and dashed lines, respectively. RMS is the root-mean-square difference between the y variate and the least-squares fit (equation on right of panel).

between peak values and the end of the growing season is considerable (e.g. 50% for Walker Branch; Fig. 5). However, we cannot expect a proportional decrease in GPP because, within the conventional (constant-$V_{cmax}^{25,toc}$) simulation, sub-optimal climatic conditions limit photosynthesis at the start and end of the growing cycle.

Implementation of a time-varying V_{cmax}^{25} based on daylength (Bonan et al., 2011; Bauerle et al., 2012) into the CLM carbon model produces a reduction in global GPP of 3–12%, which is generally below that derived above (11%). This is expected given that tropical broadleaf forest, for which V_{cmax}^{25} can be treated as relatively constant, contributes significantly to global GPP. Time-varying V_{cmax}^{25} inferred from, respectively, field measurements and remotely sensed sun-induced fluorescence has greater impact on sub-annual timescales when implemented in carbon models for Walker Branch forest (Xu and Baldocchi, 2003) and for 6 crop sites (Zhang et al., 2014). There is particularly an improvement in simulated GPP and carbon exchange against eddy covariance fluxes at the beginning and end of the growing season. We postpone a comparison of simulated/observed fluxes using different V_{cmax}^{25} formulations to a future (dedicated) study. There are a lot of parameters/processes, other than V_{cmax}^{25}, which influence simulated fluxes on sub-annual timescales (e.g. seasonal moisture stress; Baker et al., 2008; Alton, 2014). Therefore, model convergence towards observation-based fluxes might simply hide or counteract another bias/error in either the simulations or the observations.

Our results show that spatial variability is at least as important as seasonality. Thus, substantial scatter is superimposed onto the systematic reduction in Fig. 9, when introducing a $V_{cmax}^{25,toc}$ which is site-specific rather than PFT-based. Using the root-mean-square difference about the best-fits in panels (a) and (c), the impact of sub-PFT spatial variability is equivalent to 12% GPP (again excluding tropical broadleaf forest to make a fair comparison between spatial and temporal effects). The large range in Rubisco-limited photosynthetic capacity in Table 4, in particular for field measurements, also underlines the need for a sub-PFT spatial representation of this key biophysical parameter. V_{cmax}^{25} based on daylength (Bonan et al., 2011; Bauerle et al., 2012) adds some spatial differentiation according to latitude but satellite remote sensing provides even better spatial resolution.

In a very simple way, Alton (2011) introduces a 1° (<100 km) spatial heterogeneity of $V_{cmax}^{25,toc}$ into a global simulation of net primary productivity. However, no account is taken of seasonal variability within each grid square. The impact on global annual net primary productivity is only 2%, compared to a simulation adopting PFT-specific V_{cmax}^{25}. The change is modest owing to cancellation

when integrating the grid squares globally. Over 10° latitude bands, the root-mean-square difference is considerably greater (13%). Clearly, the errors in adopting a time-invariant PFT-based parameterisation of $V_{cmax}^{25,toc}$ vary in magnitude according to the spatial and temporal scale of interest. Nevertheless, they rank as moderately important in the list of quantified uncertainties in carbon modelling (Alton, 2016).

3.5. Study limitations and uncertainty analysis

One of the main objectives of the current study is to quantify the main sources of error for future improvement of the retrieval. The two main limitations of the methodology are: (1) uncertainties associated with the input remotely sensed quantities (LAI footprint/calibration and MTCI calibration against ground chlorophyll concentration); and (2) uncertainties in the adopted empirical biochemical relations which make the link between ground chlorophyll concentration and photosynthetic capacity ($J_{\max}^{25}$-V_{cmax}^{25} and $J_{\max}^{25} - Chl$). These two main limitations are treated in turn below.

Systematic errors in LAI are monitored by retrieving both with and without a site-normalisation of LAI. Except for C3 crops, they are modest at the PFT level (7% impact on retrieved median $V_{cmax}^{25,toc}$). Differences between the retrievals site-norm and site-norm-cal2 suggest a moderate sensitivity to calibration of MTCI against ground chlorophyll concentration (13% impact on retrieved median $V_{cmax}^{25,toc}$). An important further advance in using MTCI will be ground calibration for different PFTs. V_{cmax}^{25} correlates with N $(\text{vol})^{-1}$ rather than N $(\text{area})^{-1}$ owing to a higher N-use efficiency in thin, short-lived leaves compared to thick, perennial leaves (Evans, 1989; Hikosaka, 2004). This implies a sensitivity of our technique (both MTCI calibration and biochemical empirical relations) to leaf type (e.g. thick versus thin) and therefore to PFT.

The empirical relation $J_{\max}^{25}$-V_{cmax}^{25} adopted in Eq. (5) (Appendix A) appears to be fairly conservative across different PFTs (Wullschleger, 1993; Kattge et al., 2009; Walker et al., 2014), although some authors record quite high variability in the relation for different PFTs, different species and across the growing season (Meir et al., 2002; Grassi et al., 2005; Wilson et al., 2000). Our Monte-Carlo analysis suggests that uncertainty in both this and the $J_{\max}^{25} - Chl$ relation are major sources of error. The gradient of the $J_{\max}^{25} - Chl$ relation is particularly important in determining the sensitivity of retrieved $V_{cmax}^{25,toc}$ to MTCI and, therefore, the range both across the season and between sites. Currently, the positive (non-zero) intercept of the adopted $J_{\max}^{25} - Chl$ relation ($J_{\max}^{25} = 240 \times Chl + 24$) means that there is electron transport even when chlorophyll is absent and this requires verification by further leaf measurements. An important further advance would be development of a PFT-specific $J_{\max}^{25} - Chl$ relation, which may resolve differences between retrieved and field-based averages for C3 crops.

For Walker Branch, most of the uncertainty in $V_{cmax}^{25,toc}(site, month)$ (28% for the peak growing season May–August; Fig. 5) arises from uncertainties in the empirical biochemical relations. These exceed systematic errors arising from the LAI footprint/calibration and MTCI-Chl calibration. At site level, random error in input LAI mostly cancels through averaging of retrievals across MERIS years to $V_{cmax}^{25,toc}(site, month)$. Pooling and averaging of sites to PFT-level in Table 4 also largely cancels random errors in MTCI, including soil background. Although the uncertainty in our retrieval method is still large (e.g. 28% for individual sites and slightly less at PFT level), our retrieval method is still a significant advance when placed in the following context:

1. Within compilations of field observations (Wullschleger, 1993; Kattge et al., 2009; Wright et al., 2005; Beerling and Quick, 1995), ranges are large and averages sometimes differ significantly amongst themselves (often by a factor 2).
2. Most LSMs adopt time-invariant values of V_{cmax}^{25} defined per PFT. However, over the extended growing season at Walker Branch (April–Oct), retrieved $V_{cmax}^{25,toc}(site, month)$ and leaf-measured V_{cmax}^{25} change by 21 μmol m^{-2} s^{-1} and 51 μmol m^{-2} s^{-1}, respectively (Fig. 5). Thus, implementation of a seasonally dynamic Rubisco-limited photosynthetic capacity outweighs the typical systematic uncertainty in the retrieval at Walker Branch ($\pm$10–12 μmol m^{-2} s^{-1}).
3. The real advantage of our technique is the global availability of MTCI, potentially yielding $V_{cmax}^{25,toc}$ at 0.12° ($\lesssim$13 km) resolution at monthly timesteps for the whole ice-free land-surface area. This spatially explicit information provides an important new input to global carbon modelling even if a recalibration of the retrieved values is ultimately necessary against field measurements.

One advantage of our method is that, by remotely sensing chlorophyll, we obviate the potentially flawed assumption that the ratio of active leaf N (associated with $J_{\max}^{25}$ and V_{cmax}^{25}) to total leaf N (active plus structural) is constant in time (Grassi et al., 2005). This assumption is inherent in multiple regression of remotely sensed hyperspectra against measured field leaf N (e.g. Smith et al., 2002; Ollinger et al., 2013). We do, however, assume a static relationship between $J_{\max}^{25}$ and V_{cmax}^{25} across the growing season which is sometimes, but not always, confirmed in the field (Grassi et al., 2005; Wilson et al., 2000). One advantage of multiple regression techniques, over simple indices such as MTCI, is that we can use the presence of molecules other than chlorophyll (e.g. accessory pigments) to determine photosynthetic capacity.

Houborg et al. (2013) retrieve leaf chlorophyll content from broadband (rather than hyperspectral) satellite-observed reflectance and exploit empirical relationships between active and total foliar N, recorded for crops, in order to derive seasonal V_{cmax}^{25}. It is worthwhile comparing with Eqs. (3) and (5) in Appendix A which make the same connection, without reference to total N, between chlorophyll content and V_{cmax}^{25}. Thus, for a leaf chlorophyll content of 0.25–0.50 g m^{-2}, Eq. (4) and Table 2 in Houborg et al. yield 36–99 μmol m^{-2} s^{-1}. Our values from Eqs. (3) and (5) are 33–70 μmol m^{-2} s^{-1}, thus 8–29% lower. The agreement is fair given the diversity of the methods. The partitioning of active and total N by Houborg et al. applies strictly to crops but a future extension to other PFTs would provide a welcome check on our own method.

4. Summary and conclusions

We have developed a novel retrieval of top-of-canopy Rubisco-limited photosynthetic capacity (i.e. maximum carboxylation rate, $V_{cmax}^{25,toc}$) using remote sensing inputs of LAI, from MODIS, and the MERIS terrestrial chlorophyll index (MTCI). Monthly values are retrieved for the period 2003-2011 for 296 global FLUXNET sites (made available as an online catalogue) and for 8 PFTs. Our main conclusion is that $V_{cmax}^{25,toc}$ is variable both across the seasonal cycle (in time) and between sites of the same PFT (in space) and should, therefore, be incorporated *via* remote sensing into carbon model forcing.

More specifically, our findings are as follows:

1. Averaging over PFTs, our retrieved values are close to averages from field-based compilations. However, the range we retrieve per PFT for the peak growing season is smaller than that indicated by field measurements (IQR/median = 0.4, where IQR is the interquartile range, *versus* 0.5–0.7 for field compilations).
2. For all PFTs, except tropical broadleaf forest, there is a pronounced seasonal cycle in $V_{cmax}^{25,toc}$ such that photosynthetic capacity declines outside the growing season by a factor of 1.6, on average, from the peak annual value. This is true for

grasses, crops, shrubs and trees (both needleleaf and non-tropical broadleaf).

3. Uncertainty in the retrieval is large (25–30%) and stems mostly from the adopted empirical biochemical relations, particularly the link between electron transport and chlorophyll detected with the MTCI. This relation influences greatly the overall magnitude of retrieved values and the range both across the season and between sites. LAI heterogenity across the satellite footprint also leads to a comparable systematic error for C3 crops.
4. Forcing the JULES-SF land-surface model with a site-specific seasonally dynamic $V_{cmax}^{25,toc}$ reduces simulated annual GPP by 11% compared to a conventional simulation based on a seasonal constant per PFT. Moreover, the impact of sub-PFT (spatial) variability in $V_{cmax}^{25,toc}$ on GPP (12%) is as important as that of temporal variability (11%).
5. This novel remote-sensing retrieval has the potential to detect spatial and temporal variability and incorporate it into carbon models. However, better calibration of the adopted biochemical relations is required. Additional comparison against similar empirical (e.g. Houborg et al., 2013) and multiple regression hyperspectral (e.g. Smith et al., 2002; Serbin et al., 2012) methods would be beneficial in this regard.

Acknowledgements

MTCI data are provided courtesy of the NERC Earth Observation Data Centre (NEODC), ESA who provided the original data and Astrium GEO-Information Services who processed this data. We are grateful to the PIs and Co-Is of FLUXNET who make their data freely available to the ecological modelling community through the FLUXNET archive (http://FLUXNET.ornl.gov/). These contributors include, but are not limited to, Falge, E., M. Aubinet, P. Bakwin, D. Baldocchi, P. Berbigier, C. Bernhofer, A. Black, R. Ceulemans, A. Dolman, A. Goldstein, M. Goulden, A. Granier, D. Hollinger, P. Jarvis, N. Jensen, K. Pilegaard, G. Katul, P. Kyaw Tha Paw, B. Law, A. Lindroth, D. Loustau, Y. Mahli, R. Monson, P.Moncrieff, E. Moors, W. Munger, T. Meyers, W. Oechel, E. Schulze, H. Thorgeirsson, J. Tenhunen, R. Valentini, S. Verma, T. Vesala, and S. Wofsy.

Appendix A.

Measurements by several authors, compiled in Fig. 10, suggest a correlation between the maximum electron transport at a standard temperature of 25 °C ($J_{\max}^{25}$; μmol m^2 s^{-1}) and leaf chlorophyll content ($Chl(L)$; g m^{-2}). Thus:

$$J_{\max}^{25}(L) = (a_{chl} \times Chl(L)) + b_{chl} \quad (3)$$

where $Chl(L)$ is defined for a leaf located at a cumulative (i.e. from the canopy top) leaf area index equal to L. A least-square linear fit yields 240 μmol s^{-1}g^{-1} and 24 μmol m^2 s^{-1} for a_{chl} and b_{chl}, respectively, with a standard error of 16 μmol m^2 s^{-1} (13% mean $J_{\max}^{25}$). Uncertainty in this relation is quite high owing to: (1) the small number of direct measurements (most authors measure Chl versus foliar N rather than versus $J_{\max}^{25}$); and (2) the role of accessory pigments and other non-chlorophyll molecules contributing to light-harvesting and the efficiency of electron transport (Evans, 1989; Mauseth, 1998; Gurevitch et al., 2006). We take account of the standard error in our Monte Carlo uncertainty analysis.

Leaf chlorophyll content, summed over the LAI of the canopy, yields the chlorophyll concentration per unit ground which is detected by the hyperspectral satellite index MTCI. Thus:

$$\int_0^{LAI} Chl(L)dL = (a_{mtci} \times MTCI) + b_{mtci} \quad (4)$$

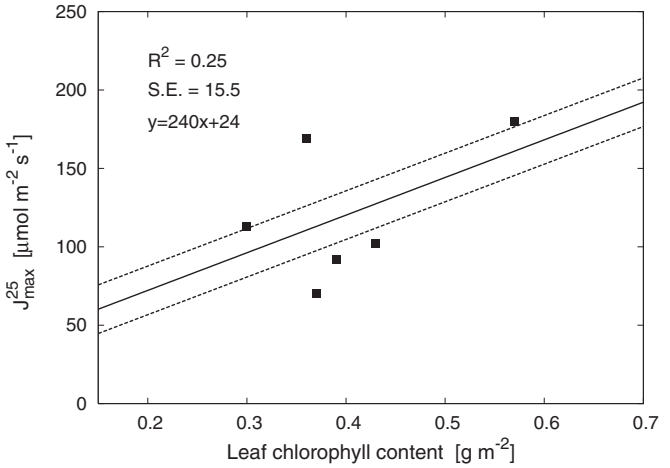

Fig. 10. The maximum electron transport at 25°C ($J_{\max}^{25}$) against leaf chlorophyll content, using measurements by Singsaas et al. (2003) for forbs, Warren et al. (2014) for sweetgum (broadleaf tree), Ripullone et al. (2003) for both Douglas fir (needleleaf tree) and poplar (broadleaf tree) and by Nolan and Smillie (1976) for barley (C3 crop). The solid line denotes a least-squares linear fit with dashed lines corresponding to the standard error of 15.5 μmol m^2 s^{-1}.

where ground calibration of cereal crops and grassland, using stratified sampling across the MERIS footprint, yields values of 0.616 g m^{-2} and −0.700 g m^{-2} for a_{mtci} and b_{mtci}, respectively (Dash et al., 2010). The correlation is strong (R^2 = 0.80) with a moderate standard error (0.052 g m^{-2} or 7% mean ground chlorophyll concentration). Note that a scaling error in Dash et al. (2010) is corrected in Eq. (4). Ideally, a calibration per PFT is preferred but this is currently unavailable (J.Dashpriv.comm.). A second MTCI-calibration is carried out by Vuolo et al. (2012) who sample a heterogeneous area in Italy, which includes forage crops and trees (fruit and poplar). Some canopy radiative transfer modelling is incorporated in order to upscale to the MERIS footprint. This calibration yields 0.469 and −0.484 for a_{mtci} and b_{mtci}, respectively (R^2 = 0.74; standard error 0.030 gm^{-2}). This alternative MTCI-calibration is implemented under the retrieval experiment site-norm-cal2 in the methodology (Section 2.3).

Many authors measure a tight, quasi-linear relation between $J_{\max}^{25}(L)$ and the maximum carboxylation rate at, or close to, the same temperature ($V_{cmax}^{25}(L)$; e.g. Wullschleger, 1993; Meir et al., 2002; Kattge et al., 2009; Walker et al., 2014). Although fitted linearly by previous authors, we find that a near-linear curve produces slightly better least-squares fit. Thus:

$$J_{\max}^{25}(L) = a_{wull}(1 - \exp(-V_{cmax}^{25}(L)/b_{wull})) \quad (5)$$

where best fit values for a_{wull} and b_{wull} are 428 μmol m^{-2} s^{-1} and 158 μmol m^{-2} s^{-1}, respectively. The standard error is low (2.3 μmol m^2 s^{-1} or 2% mean $J_{\max}^{25}$) and the relation appears quite conservative across a wide range of PFTs (Wullschleger, 1993). However, for the 3 large databases of Walker et al. (2014), Kattge et al. (2009) and Wullschleger (1993), the empirical relation fitted for $J_{\max}^{25}$-V_{cmax}^{25} differs by 12% for a_{wull} and we take account of this systematic error in our Monte-Carlo uncertainty analysis.

Several authors measure an exponential decrease in active foliar N according to leaf position, such that:

$$V_{cmax}^{25}(L) = V_{cmax}^{25,toc} \exp(-k_{rub}L) \quad (6)$$

where $V_{cmax}^{25,toc}$ is $V_{cmax}^{25}(L)$ at the canopy top and k_{rub} is the vertical N allocation parameter, for which we adopt a value of 0.15 (Carswell et al., 2000; Lewis et al., 2000; Meir et al., 2002).

To determine $V_{cmax}^{25,toc}$ for given values of MTCI and LAI, we combine the above four empirical relationships (Eq. (3–6)) in the

following way. We substitute Eqs. (6 and 3) into, respectively, the right and left of Eq. (5). Thus:

$$Chl(L) = 428[1 - (24/428) - \exp(-V_{cmax}^{25,toc} \exp(-0.15L)/158)] \quad (7)$$

where k_{rub}=0.15, a_{wull}=428, b_{wull}=158, a_{chl}=240 and b_{chl} = 24 have been substituted.

Finally, both sides of Eq. (7) are integrated with respect to cumulative leaf area L and Eq. (4) substituted into the resulting left-hand side. Using values of 0.616 and −0.700 for a_{mtci} and b_{mtci}, respectively, this yields:

$$240 \times (0.616 \times MTCI - 0.700) = \int_0^{LAI} 428 \left[1 - (24/428) - \exp\left(\frac{-V_{cmax}^{25,toc} \exp(-0.15L)}{158}\right)\right] dL \quad (8)$$

Since the integral on the right-hand side contains a double exponential function, it is solved numerically by forward modelling. A grid of $V_{cmax}^{25,toc}$ and LAI values, separated by 1 μmol m^{-2} s^{-1} and 0.01 m^2 m^{-2}, respectively, is substituted into the right side of Eq. (8) in order to create a look-up table. The intervals are sufficiently close to ensure adequate precision in the retrieval of $V_{cmax}^{25,toc}$ from given values of MTCI and LAI.

Appendix B.

The average seasonal cycle per site, $V_{cmax}^{25,toc}(site, month)$, is made available as an open database, according to the instructions below. A complete timeseries from 2003 to 2011 is not provided since noise in the input LAI timeseries makes the retrieval at monthly timesteps quite uncertain.

The average seasonal cycle is stored as a text file called <name><long><lat>.txt, where name, long and lat are the site name and coordinates given in the FLUXNET ancillary database (Agarwal, 2012). Thus, USWBW-84.29+35.96.txt corresponds to Walker Branch depicted in Fig. 5. The first three rows of the text file provide header information, viz. site ID (row 1), longitude and latitude coordinates (row 2) and column descriptors (row 3). Lines 4–15 contain a first column for month, a second column for $V_{cmax}^{25,toc}(site, month)$ from the main retrieval (site-norm), a third column for quality (Q = 1 for retrieved values, Q = 0 for missing values filled by bilinear interpolation) and finally, a fourth column for $V_{cmax}^{25,toc}(site, month)$ retrieved without site-normalisation of LAI (sat-only).

$V_{cmax}^{25,toc}(site, month)$ should be multiplied by a factor of 0.84–0.90 for carbon models requiring an average canopy value rather than a value for the canopy top. This corresponds to the point in the canopy where half the downwelling photosynthetically active radiation has been absorbed by the foliage. The assumptions are a spherical leaf angle distribution and an average diurnal solar zenith angle of 30° (×0.84) to 60° (×0.90; Campbell and Norman, 1998, p. 249).

The text files are freely available at the following internet address: http://ggluck.swansea.ac.uk/ftp/apaul. For bulk download, they can also be obtained via anonymous ftp as follows:

1. ftp ggluck.swansea.ac.uk
2. cd apaul
3. prompt
4. mget *
5. quit

References

Abramowitz, G., Leuning, R., Clark, M., Pitman, A., 2008. Evaluating the performance of land surface models. J. Climate 21, 5468–5481.

Agarwal, D. (Ed.), 2012. Biological and Ancillary Data for FLUXNET Sites, Data set. , Available at: http://www.fluxdata.org.

Alton, P., Ellis, R., Los, S., North, P., 2007. Improved global simulations of Gross Primary Product based on a separate and explicit treatment of diffuse and direct sunlight. J. Geophys. Res. 112, D07203.

Alton, P., Bodin, P., 2010. A comparative study of a multilayer and a productivity (light-use) efficiency land-surface model over different temporal scales. Agric. For. Meterol. 150, 182–195.

Alton, P., 2011. How useful are plant functional types in global simulations of the carbon, water, and energy cycles? J. Geophys. Res. (Biosci.) 116 (G1).

Alton, P., 2014. Reconciling simulations of seasonal carbon flux and soil water with observations using tap roots and hydraulic redistribution: a multi-biome FLUXNET study. Agric. For. Meteorol. 198-199, 309–319.

Alton, P., 2016. The sensitivity of models of gross primary productivity to meteorological and leaf area forcing: a comparison between a Penman-Monteith ecophysiogical approach and the MODIS Light-Use Efficiency algorithm. Agric. For. Meterol. 218-219, 11–14.

Baker, I.T., Prihodko, L., Denning, A.S., Goulden, M., Miller, S., da Rocha, H.R., 2008. Seasonal drought stress in the Amazon: reconciling models and observations. J. Geophys. Res. 113, G00B01, http://dx.doi.org/10.1029/2007JG000644.

Ball, J., Woodrow, E., Berry, J., 1987. A model predicting stomatal conductance and its contribution to the control of photosynthesis under different environmental conditions. In: Biggins, J., Nijhoff, M. (Eds.), Progress in Photosynthesis Research. Dordrecht, Netherlands, pp. 221–224.

Bauerle, W., Oren, R., Way, D., Qian, S., Stoy, P., Thornton, P., Bowden, J., Hoffman, F., Reynolds, R., 2012. Photoperiodic regulation of the seasonal pattern of photosynthetic capacity and the implications for carbon cycling. Proc. Natl. Acad. Sci. U. S. A. 109 (22), 8612–8617.

Beerling, D., Quick, W., 1995. A new technique for estimating rates of carboxylation and electron transport in leaves of C3 plants for use in dynamic global vegetation models. Glabal Chnage Biol. 1, 289–294.

Bonan, G.B., Lawrence, P.J., Oleson, K.W., Levis, S., Jung, M., Reichstein, M., Lawrence, D.M., Swenson, S.C., 2011. Improving canopy processes in the Community Land Model version 4 (CLM4) using global flux fields empirically inferred from FLUXNET data. J. Geophys. Res. 116, G02014, http://dx.doi.org/10.1029/2010JG001593.

Boyd, D., Almond, S., Dash, J., Curran, P., Hill, R., Foody, G., 2012. Evaluation of Envisat MERIS terrestrial chlorophyll index-based models for the estimation of terrestrial gross primary productivity. IEEE Geosci. Remote Sens. Lett. 9, 457–461.

Campbell, B., Norman, J., 1998. Environmental Biophysics. Springer-Verlag, New York.

Carswell, F., Meir, P., Wandelli, E., et al., 2000. Photosynthetic capacity in a central Amazonian rain forest. Tree Physiol. 20, 179–186.

Chen, J., Reynolds, J., Harley, P., Tenhunen, J., 1993. Coordination theory of leaf N distribution in a canopy. Oecologia 93, 63–69.

Clark, R.N., Swayze, G.A., Gallagher, A., King, T.V.V., Calvin, W.M., 1993. The U.S. Geological Survey, Digital Spectral Library: Version 1: 0.2 to 3.0 μm, U.S. Geological Survey, Open File Report 93-592, 1326.

Collatz, G., Ball, J., Grivet, C., Berry, J., 1991. Physiological and environmental regulation of stomatal conductance, photosynthesis and transpiration: a model that includes laminar boundary layer. Agric. For. Meteorol. 54, 107–136.

Combal, B., Baret, F., Weiss, M., Trubuil, A., Mace, D., Pragnere, A., Myneni, R., Knyazikhin, Y., Wang, L., 2003. Retrieval of canopy biophysical variables from bidirectional reflectance: using prior information to solve the ill-posed inverse problem. Remote Sens. Environ. 84, 1–15.

Curran, P., Dash, J., Lankester, T., Hubbard, S., 2007. Global composites of the MERIS Terrestrial Chlorophyll Index Int. J. Remote Sens. 28, 3757–3758.

Dang, Q., Margolis, H., Collatz, G., 1998. Parameterization and testing of a coupled photosynthesis-stomatal conductance model for boreal trees. Tree Physiol. 18, 141–153.

Dash, J., Curran, P., 2007. Evaluation of the MERIS chlorophyll index (MTCI). Adv. Space Res. 39, 100–104.

Dash, J., Curran, P.J., Tallis, M.J., Llewelyn, M., Taylor, Gail, Snoeij, P., 2010. Validating the MERIS Terrestrial Chlorophyll Index (MTCI) with ground chlorophyll content data at MERIS spatial resolution. J. Remote Sens. 31 (20), 5513–5532.

De Kauwe, M.G., Disney, M.I., Quaife, T., Lewis, P., Williams, M., 2011. An assessment of the MODIS collection 5 leaf area index product for a region of mixed coniferous forest. Remote Sens. Environ. 115, 767–780.

Doughty, C., Asner, G., Martin, R., 2011. Predicting tropical plant physiology from leaf and canopy spectroscopy. Oecologia 165, 289–299.

Ellsworth, D., 2000. Seasonal CO2 assimilation and stomatal limitations in a Pinus taeda canopy. Tree Physiol. 20, 435–445.

Evans, J.R., 1989. Photosynthesis and nitrogen relationships in leaves of C3 plants. Oecologia 78, 9–19.

Fang, H., Wei, S., Liang, S., 2012. Validation of MODIS and CYCLOPES LAI products using global field measurements data. Remote Sens. Environ. 119, 43–54.

Falge, E., Tenhunen, J., Baldocchi, D., Aubinet, M., Bakwin, P., Berbigier, P., Bernhofer, C., Bonnefond, J.-M., Burba, G., Clement, R., Davis, K., Elbers, J., Falk, M., Goldstein, A., Grelle, A., Granier, A., Gruenwald, T., Guomundsson, J.,

Hollinger, D., Janssens, I., Keronen, P., Kowalski, A., Katul, G., Law, B., Malhi, Y., Meyers, T., Monson, R., Moors, E., Munger, J., Oechel, W., Kyaw Tha Paw, U., Pilegaard, K., Rannik, U., Rebmann, C., Suyker, A., Thorgeirsson, H., Tirone, G., Turnipseed, A., Wilson, K., Wofsy, S., 2002. Phase and amplitude of ecosystem carbon release and uptake potential as derived from FLUXNET measurements. Agric. For. Meterol. 113, 75–95.
Farquhar, G., von Caemmerer, S., Berry, J., 1980. A biochemical model of photosynthetic CO_2 assimilation in leaves of C3 species. Planta 149, 78–90.
Friend, A., 2001. Modelling canopy CO_2 fluxes: are 'big-leaf' simplifications justified? Global Ecol. Biograph. 10, 603–619.
Friend, A., Arneth, A., Kiang, N., Lomas, M., Ogee, J., Roedenbeck, C., Running, S., Santaren, J., Sitch, S., Viovy, N., Woodward, I., Zaehle, S., 2007. FLUXNET and modelling the global carbon cycle. Glabal Chnage Biol. 13, 610–633.
Grassi, G., Vicinelli, E., Ponti, F., Cantoni, L., Magnani, F., 2005. Seasonal and interannual variability of photosynthetic capacity in relation to leaf nitrogen in a deciduous forest plantation in northern Italy. Tree Physiol. 25 (3), 349–360.
Gurevitch, J., Scheiner, S., Fox, G., 2006. The Ecology of Plants. Sinauer Associates, Sunderland, USA.
Han, Q., Kawasaki, T., Nakano, T., Chiba, Y., 2008. Leaf-age effects on seasonality variability in photosynthetic parameters and its relationships with leaf mass per area and leaf nitrogen concentration within a Pinus densiflora crown. Tree Physiol. 28, 551–558.
Heinsch, F., Zhao, M., Running, S., 2006. Evaluation of remote sensing based terrestrial productivity from MODIS using regional tower eddy flux network observations. IEEE Trans. Geosci. Remote Sens. 44, 1908–1925.
Hikosaka, K., 2004. Interspecific difference in the photosynthesis-nitrogen relationship: patterns, physiological causes, and ecological importance. J. Plant Res. 117, 481–494.
Houborg, R., Cescatti, A., Migliavacca, M., Kustas, W., 2013. Satellite retrievals of leaf chlorophyll and photosynthetic capacity for improved modelling of GPP. Agric. For. Meterol. 177, 10–23.
IPCC, 2013. Climate change 2013: the physical science basis. In: Stocker, T.F., Qin, D., Plattner, G.K., Tignor, M., Allen, S.K., Boschung, J., Nauels, A., Xia, Y., Bex, V., Midgley, P.M. (Eds.), Contribution of Working Group I to the Fifth Assessment Report of the Intergovernmental Panel on Climate Change. Cambridge University Press, Cambridge, UK and New York, NY, USA.
Kattge, J., Knorr, W., Raddatz, T., Wirth, C., 2009. Quantifying photosynthetic capacity and its relationship to leaf nitrogen content for global-scale terrestrial biosphere models. Glabal Chnage Biol. 15, 976–991.
Law, B., Falge, E., Gu, L., Baldocchi, D.D., Bakwin, P., Berbigier, P., Davis, K., Dolman, A.J., Falk, M., Fuentes, J.D., Goldstein, A., Granier, A., Grelle, A., Hollinger, D., Janssens, I.A., Jarvis, P., Jensen, N.O., Katul, G., Mahli, Y., Matteucci, G., Meyers, T., Monson, R., Munger, W., Oechel, W., Olson, R., Pilegaard, K., Paw U, K.T., Thorgeirsson, H., Valentini, R., Verma, S., Vesalaa, T., Wilson, K., Wofsy, S., 2002. Environmental controls over carbon dioxide and water vapour exchange of terrestrial vegetation. Agric. For. Meterol. 113, 97–120.
Lewis, J., McKane, R., Tingey, D., Beedlow, P., 2000. Vertical gradients in photosynthetic light response within an old-growth douglas-fir and western hemlock canopy. Tree Physiol. 20, 447.
Los, S., Pollack, N., Parris, M., 2000. A global 9-yr biophysical land surface dataset from NOAA AVHRR data. J. Hydrometeorol. 1, 183–199.
Mauseth, J., 1998. Botany: An Introduction to Plant Biology. Jones and Bartlett Publishers, Sudbury, USA.
McCallum, I., Wagner, W., Schmullius, C., Shvidenko, A., Obsteiner, M., Fritz, S., Nilsson, S., 2009. Satellite-based terrestrial production efficiency modelling. Carbon Balance Manag. 4, 1–14.
Medvigy, D., Jeong, S.-J., Clark, K.L., Skowronski, N.S., Schaefer, K.V.R., 2013. Effects of seasonal variation of photosynthetic capacity on the carbon fluxes of a temperate deciduous forest. J. Geophys. Res. Biogeosci. 118, http://dx.doi.org/10.1002/2013JG002421.
Medlyn, B., Robinson, A., Clement, R., McMurtie, E., 2005. On the validation of models of forest CO_2 exchange using eddy covariance data: some perils and pitfalls. Tree Physiol. 25, 839–857.
Meir, P., Kruijt, B., Broadmeadow, M., et al., 2002. Acclimation of photosynthetic capacity to irradiance in tree canopies in relation to leaf N concentration and leaf mass per unit area. Plant Cell Environ. 25, 343–357.
Melaas, E., Richardson, A., Friedl, M., Dragoni, D., Gough, C., Herbst, M., Montagnani, L., Moors, E., 2013. Using FLUXNET data to improve models of springtime vegetation activity onset in forest ecosystems. Agric. For. Meterol. 171–172, 46–56.
Middleton, E.M., McMurtrey, J.E., Entcheva Campbell, P.K., Butcher, L.M., Chappelle, E.W., 2003. Foliar reflectance and fluorescence responses for plants under nitrogen stress determined with active and passive systems. In: International Geoscience and Remote Sensing Symposium (IGARSS).
Misson, L., Tu, K., Boniello, R., Goldstein, A., 2006. Seasonality of photosynthetic parameters ina multi-specific and vertically complex forest ecosystem in the Sierra Nevada of California. Tree Physiol. 26, 729–741.
Monteith, J.L., 1965. Evaporation and environment. Symp. Soc. Exp. Biol. 19, 205–234.
Nolan, W., Smillie, R., 1976. Multi-temperature effects on Hill reaction activity of barley chloroplasts. Biochim. Biophys. Acta 440 (3), 461–475.
Ollinger, S.V., Reich, P.B., Frolking, S., Lepine, L.C., Hollinger, D.Y., Richardson, A.D., 2013. Nitrogen cycling, forest canopy reflectance, and emergent properties of ecosystems. Proc. Natl. Acad. Sci. U.S.A. 110 (27), E2437.
Reichstein, M., Tenhunen, J., Roupsard, O., 2003. Inverse Modelling of seasonal drought effects on canopy CO_2/H_2O exchange in three Mediterranean ecosystems. J. Geophys. Res. 108, 4726, D23.
Richardson, A., Williams, M., Hollinger, D., Moore, D., Dail, D., Davidson, E., Scott, N., Evans, R., Hughes, H., Lee, J., Rodrigues, C., Savage, K., 2010. Estimating parameters of a forest ecosystem C model with measurements of stocks and fluxes as joint constraints. Oecologia 164, 25–40.
Ripullone, F., Grassi, G., Lauteri, M., Borghetti, M., 2003. Photosynthesis-nitrogen relationships: interpretation of different patterns between *Pseudotsuga menziesii* and *Populus euroamericana* in a mini-stand experiment. Tree Physiol. 23, 137–144.
Running, S., Baldocchi, D., Turner, D., Gower, S., Bakwin, P., Hibbard, K., 1999. A global terrestrial monitoring network integrating tower fluxes, flask sampling, ecosystem modelling and EOS satellite data. Remote Sens. Environ. 70, 108–127.
Ryu, Y., Baldocchi, D., Kobayashi, H., van Inge, C., Lie, J., 2011. Integration of MODIS land and atmosphere products with a coupled-process model to estimate gross primary productivity and evapotranspiration from 1 km to global scales. Global Biogeochem. Cycles 25 (4), GB4017.
Sato, H., Ito, A., Ito, A., Ise, T., Kato, E., 2015. Current status and future of land surface models. Soil Sci. Plant Nutr. 61, 34–47.
Schulze, E-D., Kelliher, F., Korner, C., Lloyd, J., Leuning, R., 1994. Relationships among maximum stomatal conductance, ecosystem surface conductance, carbon assimilation rate and plant N nutrition: a global ecology scaling exercise. Annu. Rev. Ecol. Syst. 25, 629–660.
Sellers, P., Randall, D., Collatz, G., et al., 1996. A revised land surface parameterization (SiB2) for atmospheric GCMs. Part I: Model formulation. J. Climate 9, 676–705.
Serbin, S., Dillaway, D., Kruger, E., Townsend, P., 2012. Leaf optical properties reflect variation in photosynthetic metabolism and its sensitivity to temperature. J. Exp. Bot. 63, 489–502.
Serbin, S., Ahl, D., Stith, G., 2013. Spatial and temporal validation of the MODIS LAI and FPAR products across a boreal forest wildfire chronosequence. Remote Sens. Environ. 133, 71–84.
Shabanov, N., Huang, D., Yang, W., Tan, B., Knyazikhin, Y., Myneni, R., Ahl, D., Gower, S., Huete, A., Arago, L.-E., Shimabukuro, Y., 2005. Analysis and Optimization of the MODIS Leaf Area Index Algorithm Retrievals Over Broadleaf Forests.
Sheffield, J., Goteti, G., Wood, E., 2006. Development of a 50-year high-resolution global dataset of meteorological forcings for land surface modeling. J. Clim. 19, 3088–3111.
Singsaas, E., Ort, D., DeLucia, E., 2003. Elevated CO_2 effects on mesophyll conductance and its consequences for interpreting photosynthetic physiology. Plant Cell Environ. 27, 41–50.
Smith, M-L., Ollinger, S., Martin, M., Aber, J., Hallett, R., Goodale, C., 2002. Direct estimation of aboveground forest productivity through hyperspectral remote sensing of canopy nitrogen. Ecol. Appl. 12 (5), 1286–1302.
Vina, A., Gitelson, A., Nguy-Robertson, A., Yi, P., 2011. Comparison of different vegetation indices for the remote assessment of green leaf area index of crops. Remote Sens. Environ. 115, 3468–3478.
Vuolo, F., Dash, J., Curran, P., Lajas, D., Kwiatkowska, E., 2012. Methodologies and uncertainties in the use of the Terrestrial Chlorophyll Index for the Sentinel-3 mission. Remote Sens. 4, 1112–1133.
Walker, A.P., Beckerman, L., Gu, J., Kattge, L.A., Cernusak, T.F., Domingues, J.C., Scales, G., Wohlfahrt, S.D., Wullschleger, F.I., Woodward, 2014. The relationship of leaf photosynthetic traits to leaf nitrogen, leaf phosphorus, and specific leaf area: a meta-analysis and modeling study. Ecol. Evol. 4, 3227–3235.
Wang, Y., Baldocchi, D., Leuning, R., Falge, E., Vesala, T., 2007. Estimating parameters in a land-surface model by applying nonlinear inversion to eddy covariance flux measurements from eight FLUXNET sites. Glabal Chnage Biol. 13, 652–670.
Warren, J.M., Jensen, A.M., Medlyn, B.E., Norby, R.J., Tissue, D.T., 2014. Carbon dioxide stimulation of photosynthesis in Liquidambar styraciflua is not sustained during a 12-year field experiment. AoB Plants 7, http://dx.doi.org/10.1093/aobpla/plu074.
Williams, M., Richardson, A.D., Reichstein, M., Stoy, P.C., Peylin, P., Verbeeck, H., Carvalhais, N., Jung, M., Hollinger, D.Y., Kattge, J., Leuning, R., Luo, Y., Tomelleri, E., Trudinger, C.M., Wang, Y.-P., 2009. Improving land surface models with FLUXNET data. Biogeosciences 6 (7), 1341–1359.
Wilson, K., Baldocchi, D., Hanson, P.J., 2000. Spatial and seasonal variability of photosynthetic parameters and their relationship to leaf nitrogen in a deciduous forest. Tree Physiol. 20 (9), 565–578.
Wilson, K., Baldocchi, D., Hanson, P., 2001. Leaf age affects the seasonal pattern of photosynthetic capacity and net ecosystem exchange of carbon in a deciduous forest. Plant Cell Environ. 24, 571–583.
Wright, I., Reich, P.B., Cornelissen, J.H., Falster, D.S., Garnier, E., Hikosaka, K., Lamont, B.B., Lee, W., Oleksyn, J., Osada, N., Poorter, H., Villar, R., Warton, D.I., Westoby, M., 2005. New Phytol. 166 (2), 485–496.
Wullschleger, S., 1993. Biochemical Limitations to Carbon Assimilation in C3 Plants – a retrospective analysis of the A/Ci curves from 109 species. J. Exp. Biol. 44, 907–920.
Xu, L., Baldocchi, D., 2003. Seasonal trends in photosynthetic parameters and stomatal conductance of blue oak (*Quercus douglasii*) under prolonged summer drought and high temperature. Tree Physiol. 23, 865–877.

Yang, W., Tan, B., Huang, D., Rautiainen, M., Shabanov, N., Wang, Y., Privette, J., Huemmrich, K., Rasmus Fensholt, R., Sandholt, I., Weiss, M., Ahl, D., Gower, S., Nemani, R., Knyazikhin, Y., Myneni, R., 2006a. MODIS leaf area index products: from validation to algorithm improvement. IEEE Trans. Geosci. Remote Sens. 44, 1885–1898.

Yang, W., Shabanov, N.V., Huang, D., Wang, W., Dickinson, R.E., Nemani, R.R., Knyazikhin, Y., Myneni, R.B., 2006b. Analysis of leaf area index products from combination of MODIS Terra and Aqua data. Remote Sens. Environ. 104 (3), 297–312.

Yuan, W., Liu, S., Zhou, G., 2007. Deriving a light-use efficiency model from eddy covariance covariance flux data for predicting daily gross primary production across biomes. Agric. For. Meterol. 143, 189–207.

Zaehle, S., Sitch, S., Smith, B., Hatterman, F., 2005. Effects of parameter uncertainties on the modeling of terrestrial biosphere dynamics. Global Biogeochem. Cycles 19, GB3020.

Zhao, M., Heinsch, F., Nemani, R., Running, S., 2005. Improvements of the MODIS terrestrial gross and net primary production global data set. Remote Sens. Environ. 95, 164–176.

Zhang, Y., Guanter, L., Berry, J.A., Joiner, J., van der Tol, C., Huete, A., et al., 2014. Estimation of vegetation photosynthetic capacity from space-based measurements of chlorophyll fluorescence for terrestrial biosphere models. Glabal Change Biol. 20, 3727–3742.